School of Industrial and Information Engineering
Master of Science in Engineering Physics

POLITECNICO
MILANO 1863

# Characterization of Spin-Orbit Torque in single layer of compensated ferrimagnetic half-metallic material $Mn_2Ru_xGa$

**Supervisor: Prof Riccardo Bertacco**
**Co-supervisor: Prof. Michael Coey**
**Co-supervisor: Dr. Karsten Rode**

**Candidate:**
**Lorenzo Locatelli,**
**ID number: 884609**

**Accademic Year 2018-2019**

Trinity College Dublin
Coláiste na Tríonóide, Baile Átha Cliath
The University of Dublin

*The whole work presented here was carried out in the Physics and Engineering Department of Trinity College Dublin, in the Magnetism and Spin Electronics group, under the supervision of Dr. Karsten Rode.*

MAGNETISM &
SPIN ELECTRONICS
TRINITY COLLEGE, DUBLIN

*Alla mia famiglia, a Francesca, ai miei amici.*

# Abstract

During the last years, Spin-Orbit Torque (SOT) has been considered as one the most promising effect to boost the integration of spintronics into classical electronics.
In the present work, it is studied from an experimental point of view a peculiar manifestation of SOT, which happens in single layer of $Mn_2Ru_xGa$ (MRG), a ferrimagnetic, half metallic compensated material. Due to the particular symmetry of its crystal, in MRG films it is self-induced an additional polarization of the current. Such polarization is non-collinear with the magnetization, thus it exerts a torque on the magnetic moments of the lattice.
In order to investigate SOT it was studied the change of the out of plane magnetization induced by the injection of an high current density.
This out of plane magnetization was tracked exploiting the Anomalous Hall Effect (AHE), recording the transversal Hall voltage arising from the injection of a longitudinal current. Initially, it was studied the low current regime, in which the extra polarization of the flowing electrons is assumed to be linear as a function of the current density. In this regime the study was focused on the estimation of field-like and damping-like parameters, which relate the current density with the effective Spin-Orbit field.
Once estimated those two parameters, the current density was further increased and a strongly non-linear behavior was observed. In this regime SOT effect is huge, it almost switches the magnetization of the sample when the current density approaches the limit value sustainable by the device.
The investigation of SOT effect in ferrimagnets or antiferromagnets is particularly interesting because it is the most effective way to excite a dynamics in these materials, which are weakly sensitive to a magnetic field. The huge interest that is growing around exciting a dynamics in such materials is due to the fact that they possess a resonance frequency which lies in the terahertz range. Nowadays, it does not exist an electronics device which is able to operate in the terahertz range so it would be a breakthrough to engineer a device based on MRG to be integrated into classical electronics.

# Sommario

Nel corso degli ultimi anni gli effetti di Spin Orbit Torque (SOT) sono stati fra i candidati più promettenti per promuovere l'integrazione della spintronica nel mondo dell'elettronica tradizionale.
Nel presente lavoro è stata studiata una particolare manifestazione dell'effetto di SOT osservabile in film sottili di $Mn_2Ru_xGa$ (MRG), un 'ferrimagnetic, compensated half-metal'. Grazie alla particolare simmetria del suo reticolo cristallino, si riscontra che lo scorrere di una corrente attraverso tale materiale da luogo alla generazione di una ulteriore polarizzazione, auto-indotta dalla corrente stessa. Dal momento che tale extra-polarizzazione non è parallela alla magnetizzazione del materiale essa esercita un momento torcente sui dipoli magnetici del reticolo. Per investigare tali effetti di SOT è stata studiata la variazione della magnetizzazione in funzione della densità di corrente iniettata nel film. La magnetizzazione è stata rilevata sfruttando l'Anomalous Hall Effect (AHE). Tale effetto consiste nella spontanea generazione di una differenza di potenziale perpendicolare alla direzione della corrente e proporzionale alla magnetizzazione 'out of plane'. Inizialmente la corrente è stata mantenuta al di sotto di un certo livello, in modo da ottenere una relazione lineare tra la densità di corrente e la polarizzazione auto-indotta. In questo regime sono stati ricavati i due parametri fondamentali che definiscono tale relazione.
Durante la seconda parte del lavoro la densità di corrente invece è stata aumentata fino a rendere possibile l'osservazione di forti non-linearità nell'effetto di SOT, visibili chiaramente dalla variazione della magnetizzazione indotta da densità di corrente elevate.
Lo studio degli effetti di SOT in ferrimagneti e antiferromagneti è di particolare importanza in quanto tali effetti rappresentano il modo più efficace di eccitare una dinamica della magnetizzazione in questi materiali. Tale interesse è dovuto al fatto che essi possiedono una frequenza di risonanza nel range dei terahertz. Dispositivi operanti a tale frequenza rivoluzionerebbero il mondo dell'elettronica tradizionale permettendoci di creare processori sempre più veloci e performanti.

# Contents

# Chapter 1

# Introduction

During the last century information technology has been the leading actor in driving the revolution of our lifestyle. In 1941 the first computer was assembled and exploited by England to decode some encrypted German message during the second world war. Today we have the power to perform calculations that allow us to investigate branches of science that had not even been discovered some years ago. We can exploit artificial intelligence and machine learning to self-drive car and airplane. We are all simultaneously connected through the internet, and we can share each other information almost instantaneously. During the last years, researchers and industries are pushing the limits of this technology based on conventional electronics to a saturation point in terms of speed, power and dimension.
Modern branches of theoretical and experimental physics are investing much effort in order to find an alternative to conventional electronics doing research about new materials and new technologies able to replace or integrate the present one and to overcome its limits.
Among these, spin electronics has emerged in the second half of the past century as a strong candidate to implement innovative device. These can exploit the spin state of electrons as an additional degree of freedom to process and storage information.

## 1.1 Electrically driven magnetic excitation

Initially, spin electronics was mainly based on ferromagnetic materials and took advantage of their sensitivity to a magnetic field to give rise to particular magnetoresistance effect when coupled with non magnetic materials [1] or oxides [2].

Later, in 1996, it was proposed, independently by Slonczewski [3] and Berger [4] the possibility to excite the magnetization of a material employing a polarized current flowing into it, instead of using an external magnetic field. These studies had an enormous scientific and technological impact because such a spin-transfer mechanism would make it possible to avoid the use of a magnetic field in spintronics application. A few years later it was unambiguously demonstrated that the flow of a polarized current into a ferromagnetic material was able to excite and control its magnetization through the above cited Spin Transfer mechanism [5][6].

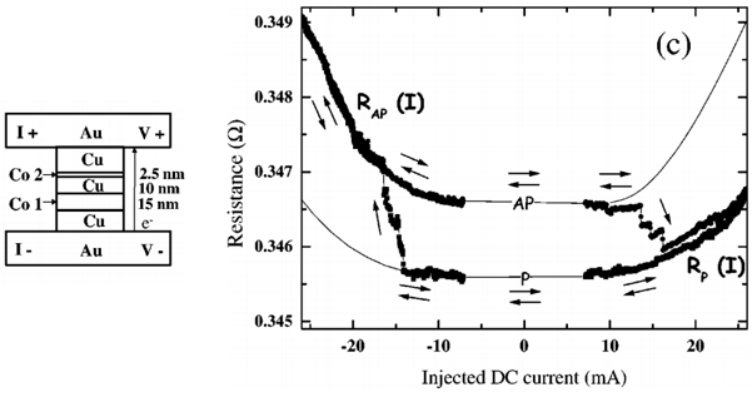


Figure 1.1: Scheme of the heterostructure on the left and result of a GMR measurement on the right. A non-magnetic layer of Copper separates the two magnetic layers of Cobalt. The current flows perpendicular to the plane of the films and depending on the sign and intensity of the injected current one of the two layers eventually switches.

The first configuration used to control the magnetization of a material electrically is shown in figure 1.1, it consists in employing a three-layer structure in which two magnetic layers are separated by a non-magnetic one or an oxide. The current flowing through the first magnetic layer is polarized, and it gains an angular momentum which then will be transferred to the second layer.
This phenomenon was the first step into the branch of electrical control of magnetization in magnetic materials, since that moment a lot of different methods and configuration of the heterostructure were tested to improve the efficiency of those devices.
An important step forward in this direction was achieved when the polarization of the current was for the first time achieved exploiting Spin-Orbit

Interaction. In particular, Spin Hall Effect (SHE) [7], was exploited to convert a charge current into a spin current, perpendicular to the initial one. This effect is related to Spin-Orbit Interaction; thus, it is effective in heavy metal such as Platinum or Tantalum. It consists into an asymmetric scattering probability for electrons with a different spin orientation, if the spin current is then directed toward an adjacent magnetic layer it can change the equilibrium position of the magnetization [8] or eventually excite a particular dynamics [9].

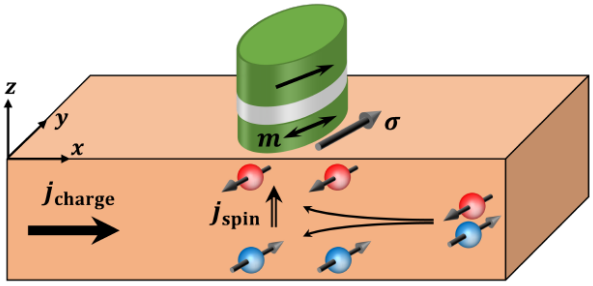


Figure 1.2: Representation of the scheme used to control the magnetization of a free layer through Spin-Hall Effect. Integrated with this device, there is also a magnetic tunnel junction employed to detect the orientation of the free layer.

In the configuration shown in figure 1.2 the switch of the free layer is achieved through the spin-charge that is accumulated at the interface between the Spin-Hall metal and the ferromagnetic material above it. The main advantage is that in this configuration the current needed to switch the free layer has to flow in the heavy metal below the free layer, not through the magnetic tunnel junction itself, which is exploited just to read the orientation of the free layer.
Beyond this application, the generation of a polarized current through the use of SHE could also be employed to excite particular dynamics in ferromagnet placed above it [9].

## 1.2 New magnetic materials

In this scenario, it grows the need of studying new magnetic materials, such as antiferromagnets to be integrated with those emerging methods of electrically control the magnetic state of materials.

Antiferromagnets are magnetic materials with a zero net magnetization resulting from the antiparallel alignment of their ionic magnetic moment. They had a marginal role in spin electronics research and technology until very recent years, and this could be understood because of the evident difficulty in controlling them exploiting magnetic fields.
On the other hand, they present interesting properties such as an extremely high resonance frequency and the complete absence of a stray field which, from a technological point of view, imply high speed and good scalability.
This need of combining high spin polarization with some promising properties of antiferromagnets, such as high speed and good scalability, was eventually met in 2014 by H. Kurt [10]. It was for the first time fabricated an half-metallic, compensated ferrimagnet in the spin electronics group of Trinity College Dublin as $Mn_2Ru_xGa$ (MRG).
Such material is composed by two ferromagnetic sublattices, antiferromagnetically coupled each other and crystallographically inequivalent.
These properties result in the fact that being inequivalent, just one of the two sublattices participates to transport phenomena, implying a high spin polarization, and, on the other hand, high speed dynamics, good scalability and robustness against external magnetic fields.

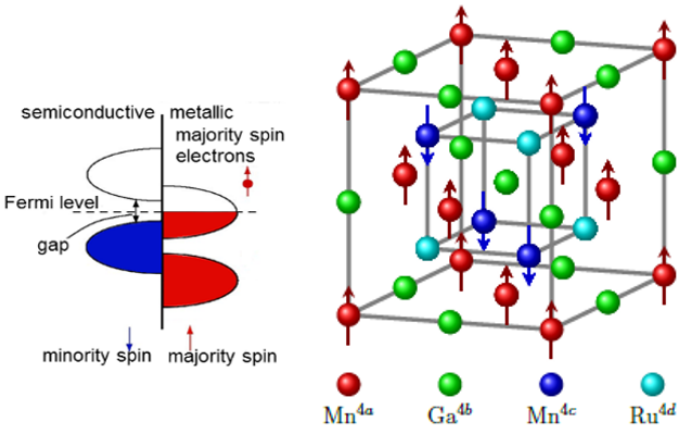


Figure 1.3: Schematic representation of the band structure of an half-metal on the left and of the crystal structure of MRG on the right.

Such material showed a polarization of the electric current flowing into it which is comparable with the polarization obtained in a conventional ferromagnets and, simultaneously, a zero net magnetization. The combination of these two properties makes it one of the most promising materials for the

realization of spintronics devices and their integration into conventional electronics.
Moreover, after theoretical study about the relation between the symmetry of crystals and their transport properties [11] it was predicted that the symmetry point group of such a material implies a polarization of the current which is not collinear with the direction of the magnetization; thus it exerts a torque on it.
Since this effect is driven by Spin-Orbit interaction, this torque is addressed as Spin-Orbit Torque (SOT), but it has not to be confused with the abovecited torque induced by spin Hall effect in heavy metal. In this case, there is no need for an extra layer to generate a spin current; the polarization is induced by the current itself because it flows into such a lattice.
This thesis is mainly devoted to investigating this torque exerted by a polarized current on the magnetization of the material. Moreover, the orientation of this polarization directly depends on the direction of the magnetization so an interesting dynamics could also be expected because if the magnetization is exited and changes its orientation also the polarization has to evolve.

## 1.3 Summary and outlook of the thesis

This thesis project has been developed in the Magnetism and spin electronics group of Trinity College Dublin (TCD) headed by professor M.J.D. Coey and under the direct supervision of senior researcher Dr. Karsten Rode. During the time spent there, I took part in a project focused on the study of Spin-Orbit Torques in single layers of a ferrimagnetic, half-metallic, compensated material, namely $Mn_2Ru_xGa$ (MRG).
When I joined the group, SOT effect had already been observed for the first time in a single layer of MRG. I participated in the investigation of such an effect trying to gain a deeper understanding of this phenomena from a physical point of view.
The work was carried out with a strong experimental character, and I had access to all the facilities present in SNIAM and CRANN laboratories in Trinity College.
The thesis could be divided into three main parts. During the first period, I was involved in measurements that were carried out to characterize the linear part of SOT in a single layer of MRG. During this part, I was mainly trained in the use of the experimental setup, and I had the time to understand how to perform transport experiment in a helium flow cryostat independently and to study the literature about SOT and MRG.

The second part of the work was oriented to the general characterization of a new sample, that was fabricated before I started my research experience in TCD. The aim was to verify that it was a suitable sample to continue the research about SOT previously started. During this part of the thesis, I initially characterized the sample from a crystallographic point of view to verify that it was correctly grown, then I proceeded with some rough magneto-transport measurement to verify that also from a magnetic point of view the sample was behaving as expected.
After this verification, the sample was divided into two pieces. These have been patterned in a different way to create two devices, both with a Hall bar geometry, but the current path rotated of $45^o$.
The patterned devices were then properly characterized with magneto-transport measurement, compensation temperature, coercitivity and anisotropy constant were estimated.
The third part of the thesis was then devoted to the SOT characterization in the non-linear current regime. These measurements represent the core of the work because a completely new effect was studied, along two different directions of the current. The whole experiment was performed at room temperature and atmospheric pressure, and then the results were analyzed also taking into account the temperature behavior previously measured. Finally SOT effect was quantified through a model developed during that period.

# Chapter 2

# Theoretical background

## 2.1 Magnetism and magnetic materials

Electromagnetism is the branch of physics devoted to the study of electromagnetic interaction, this interaction occurs between electrically charged particles and is one of the four fundamental interactions that pervade our universe.
Electromagnetism has been rather a mysterious field until the beginning of XIX century, in particular, before that period electric and magnetic interaction were considered two completely different and unrelated interactions.
Here is collocated the fundamental work of a lot of great scientists among which H. C. Orsted, C. F. Gauss, A. M. Ampère, M. Faraday and J. C. Maxwell that cooperated to the development of a classical theory able to describe electric and magnetic forces as they actually are: two different manifestation of the same interaction [12].
In this section an overview about magnetic phenomena is given, because of the experimental character of this work, particular attention is reserved to magnetism in condensed matter and its implication.

### 2.1.1 Magnetic field and magnetic energy

The expression of electric and magnetic force acting on a charged particle is expressed, as often happens in physics, by means of two corresponding electric **E** and magnetic **B** field [13].

$$\mathbf{F} = q(\mathbf{E} + \mathbf{v} \times \mathbf{B}) \tag{2.1.1.1}$$

This is the Lorentz equation for the force acting on a charged particle moving into an electromagnetic field.

In this equation electric and magnetic fields are treated as two unrelated fields, however, observing the Maxwell equations it could be understood how they always are dynamically coupled.

$$\nabla \cdot \mathbf{D} = \rho_v \tag{2.1.1.2}$$

$$\nabla \cdot \mathbf{B} = 0 \tag{2.1.1.3}$$

$$\nabla \times \mathbf{E} = -\frac{\partial \mathbf{B}}{\partial t} \tag{2.1.1.4}$$

$$\nabla \times \mathbf{H} = \mathbf{J} + \frac{\partial \mathbf{D}}{\partial t} \tag{2.1.1.5}$$

This is the version of the Maxwell equation in matter in which it appears also the vector $\mathbf{D}$ and $\mathbf{H}$ that take into account the electromagnetic properties of the material itself.

$$\mathbf{D} = \epsilon_0 \mathbf{E} + \mathbf{P} \tag{2.1.1.6}$$

$$\mathbf{H} = \frac{1}{\mu_0}\mathbf{B} - \mathbf{M} \tag{2.1.1.7}$$

In equation 2.1.1.6 and 2.1.1.7 could be noticed how the effect of polarization ($\mathbf{P}$) and magnetization ($\mathbf{M}$) strongly influences the electromagnetic behavior of materials.
It is easy to understand how crucial is the role of Magnetization in the study of magnetism in condensed matter. Its dependence from the applied magnetic field is very different as a function of the type of magnetic material that is considered.
Before going through the analysis of the different types of magnetism is useful to understand how the magnetic field is related to the flow of an electrical current.
Observing the second Maxwell equation and exploiting the divergence theorem it is easy to understand that the flux of $\mathbf{B}$ across a closed surface is always null, physically it means that the existence of a magnetic monopole is forbidden.
It is possible to do another important observation looking to the 'in vacuum' version ($\mathbf{M} = 0$) of the fourth Maxwell equation also called Ampère's law. Starting from that and exploiting the Stokes theorem it can be obtained the expression of the magnetic field generated in the geometric center of a current loop:

$$\mathbf{H} = \frac{I}{2R} \tag{2.1.1.8}$$

This expression is of crucial importance in the understanding of magnetic phenomena because it states the fundamental equivalence between a current loop and a magnetic dipole which will be exploited in the derivation of the

magnetic moment generated in an atom.
Since from the second Maxwell equation it could be derived that the existence of magnetic monopole is forbidden the simplest magnetic object that we can imagine is a dipole. The field generated by such a dipole $\boldsymbol{\mu}$ has the same shape of the electric field generated by an electric dipole.

$$\mathbf{B}(\mathbf{r}) = \frac{\mu_0}{4\pi}\left(\frac{3\mathbf{r}(\boldsymbol{\mu}\cdot\mathbf{r})}{r^5} - \frac{\boldsymbol{\mu}}{r^3}\right) \tag{2.1.1.9}$$

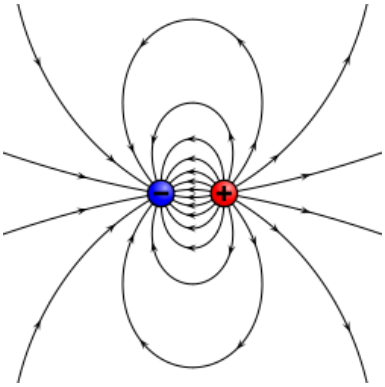

Figure 2.1: Field lines generated by a magnetic dipole

Proceeding with the formal analogy between magnetic and electric field we can write down the expression of the energy of a magnetic dipole into a magnetic field [14].

$$E = -\boldsymbol{\mu}\cdot\mathbf{B} \tag{2.1.1.10}$$

From the expression of this energy it can be understood that if the field is uniform there is not a net force exerted on the magnetic moment, i.e. the position of the dipole is not perturbed by the presence of the field.
On the other hand the way in which a magnetic field interacts with a magnetic dipole is exerting a torque on it inducing a precession of the dipole itself around the field direction.

$$\mathbf{T} = \boldsymbol{\mu}\times\mathbf{B} \tag{2.1.1.11}$$

As can be noticed from the expression of the torque it is null if the dipole is already aligned with the magnetic field. Obviously considering a realistic situation in which a moment is not completely free and isolated but it belongs to a lattice of a certain magnetic material this precession will be damped by all the other interaction present into the solid and finally the moment will be aligned toward the direction of the field.

### 2.1.2 Atomic magnetism

Considering the classical Bohr model for an atom of dimension $r$ we can easily calculate the equivalent current generated by the motion of an electron around the nucleus with period $T$ and velocity $v$.

$$I = \frac{-e}{T} = \frac{-ev}{2\pi r} = \frac{-em_e vr}{2\pi m_e r^2} = \frac{-e|\mathbf{L}|}{2\pi m_e r^2} \tag{2.1.2.1}$$

Where the last expression has been manipulated in order to show the classical electronic angular momentum, referred to the nucleus, because it will be straightforward to switch from a classical to a quantum definition of this operator [15].
Comparing the expression of the field generated by a magnetic dipole with the field due to a current loop we can easily find the expression of the magnetic dipole in terms of the area of the current loop and the current flowing into it.

$$\boldsymbol{\mu} = IA\hat{\mathbf{n}} \tag{2.1.2.2}$$

Where $\hat{n}$ is a unitary vector normal to the surface of the loop and pointing towards the direction indicated by the right hand rule.
Replacing $I$ with the expression of the current due to an electron in orbit around an atom in the Bohr model framework we find the expression of an atomic magnetic dipole.

$$\boldsymbol{\mu}_l = IA\hat{\mathbf{n}} = \frac{-e}{2m_e}\mathbf{L} \tag{2.1.2.3}$$

With this expression of the magnetic dipole moment it is possible to, easily, switch to a quantum description of the phenomena using instead of $\mathbf{L}$ the corresponding quantum operator and than its own eigenvalue.

$$\boldsymbol{\mu}_l = \frac{-e}{2m_e}\hat{\mathbf{L}} = \frac{-e\hbar}{2m_e}m_l\hat{\mathbf{n}} \tag{2.1.2.4}$$

The quantization of the angular moment directly implies the quantization of the magnetic dipole moment, which is then naturally expressed as a multiple of its smallest quantized value, named Bohr magneton $\mu_B$.

$$\boldsymbol{\mu}_l = \frac{-e\hbar}{2m_e}\hat{\mathbf{L}} = -\frac{\mu_B g_l}{\hbar}\hat{\mathbf{L}} \quad ; \quad \mu_B = \frac{e\hbar}{2m_e} \tag{2.1.2.5}$$

Where $g_l$ in this case is equal to one, but in order to be consistent with the rest of the discussion is kept as a parameter.
Considering now that an electron has also an intrinsic angular moment called

spin $\hat{\mathbf{S}}$ we expect that, as stated in equation 2.1.2.5, it possesses also a magnetic moment.

$$\boldsymbol{\mu}_s = -\frac{\mu_B g_s}{\hbar}\hat{\mathbf{S}} \tag{2.1.2.6}$$

Where $g_s$ was experimentally determined and then confirmed by Dirac's theory being approximately two. It can be stated thus that electron in an atom with a non null angular momentum possess a magnetic moment due to its spin angular moment and another one due to its orbital angular moment. The interaction between the two above quantities is called Spin Orbit Interaction (SOI) and leads to a modification of the total energy due to the coupling of angular and spin momentum.

### 2.1.3 Spin Orbit Interaction

In order to understand how the Spin Orbit Interaction influences the total Hamiltonian we choose our reference frame to be consistent with the position of an electron. Then, calculating the magnetic field produced on it by the motion of the nucleus, we can understood how the energy of the electron is modified by the presence of this magnetic field.
The coupling energy between a field and a magnetic moment is showed in equation 2.1.3.1.

$$\Delta E = -\boldsymbol{\mu} \cdot \mathbf{B} \tag{2.1.3.1}$$

This equation states that the most favorable energetic situation is reached when the magnetic dipole is parallel to the direction of the magnetic field.
In the rest frame of the nucleus the electron feels an electric field that bounds it to the atom, but due to the relativistic equivalence between electric and magnetic field in the rest frame of the electron this electric field is converted into a magnetic field.

$$\mathbf{B} = -\frac{\mathbf{v} \times \mathbf{E}}{c^2} \tag{2.1.3.2}$$

Where $\mathbf{v}$ is the electron velocity and $\mathbf{E}$ is the electric field due to the nucleus. Assuming that the electric field is radial we can write it as $\mathbf{E} = |E||\mathbf{r}/r$, and then substituting the velocity with the linear momentum it is possible to rearrange the equation in a more significant way [14].

$$\mathbf{B} = \frac{\mathbf{r} \times \mathbf{p}}{m_e c^2}\frac{|E|}{r} = \frac{1}{m_e e c^2}\frac{1}{r}\frac{\partial U(r)}{\partial r}\mathbf{L} \tag{2.1.3.3}$$

Where it has been exploited the relation between the electric field and the potential $U$: $E = -\nabla \mathbf{U}/e$. Using this definition of $\mathbf{B}$ in the equation 2.1.3.2

and considering the expression of the magnetic dipole due to the spin angular momentum we obtain:

$$\Delta E = \frac{2\mu_B}{\hbar m_e e c^2} \frac{1}{r} \frac{\partial U(r)}{\partial r} \mathbf{L} \cdot \mathbf{S} \tag{2.1.3.4}$$

This equation states that the energy of the electron in an atom depends on the relative orientation of its angular and spin momentum. Spin Orbit Interaction has a crucial role also in the perturbation of the energy bands in solids since each Bloch orbital is described by a linear combination of atomic orbital so it preserves an orbital character and thus its energy and properties are affected by SOI.

### 2.1.4 Types of magnetism

In the previous section it has been treated magnetism in isolated atoms, when atoms bound each other to generate condensed matter the magnetic properties of each single atom contribute to the magnetic properties of the macroscopic material.
There mainly exist five different types of magnetic materials: diamagnetic, paramagnetic, antiferromagnetic, ferrimegnetic and ferromagnetic.

The first type are diamagnetic materials, those materials experience a weak repulsive force when they are exposed to a magnetic field, this repulsive force is due to the fact that those materials respond to an external magnetic field generating an internal field which has an opposite direction with respect to the applied one.
All the materials posses a small diamagnetic character, this could be classically explained remembering that each current loop maintains constant the magnetic flux through its boundary, so if an external magnetic field is applied the material responds generating an internal field equal and opposite to the external one (see figure 2.2). This obviously is just an intuitive explanation of the phenomena, is well known that the right approach to explain magnetism in condensed matter shall not ignore the quantum nature of the atomic magnetic moment.
In general this effect generates a very weak interaction and in the presence of any of the other collective magnetic phenomena it becomes negligible [14].

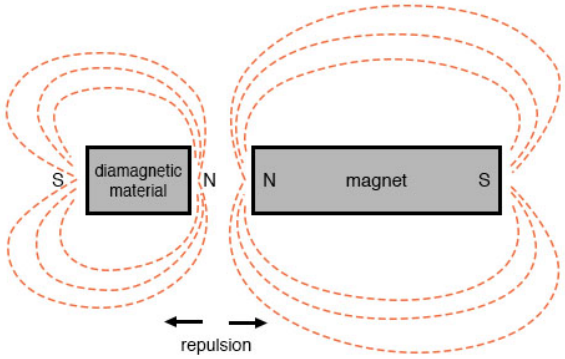


Figure 2.2: Schematic representation of the field lines induced by the presence of a magnetic field close to a diamagnetic material.

Paramagnetic materials are materials that under the effect of a magnetic field are weakly attracted towards it. Paramagnetism exists just in atoms that have an unpaired electron, i.e. in atoms that have a finite and non null magnetic moment. Without an external magnetic field applied to these atoms the direction of the magnetic dipole moment of each atom is randomly distributed in all the possible directions but if a magnetic field is applied due to equation 2.1.3.1 it defines a low energy direction for the orientation of all the dipoles.
Since the energy difference between parallel and antiparallel orientation is: $\Delta E = |\mu||B|$, increasing the magnetic field the parallel orientation becomes more energetically favorable. Obviously this phenomena is in competition with the thermal energy which tends to randomly orients the moments.
This explanation of the phenomena implies that there is a field value at which the magnetization saturates and this field is achieved when all the magnetic moments are aligned each other towards the field direction. The value of the field which is necessary to align all the magnetic moments depends on the external temperature, the magnetic energy gained at saturation should be well above the Boltzman thermal energy $\propto k_B T$ in order to be effective against energy oscillation due to temperature [16].

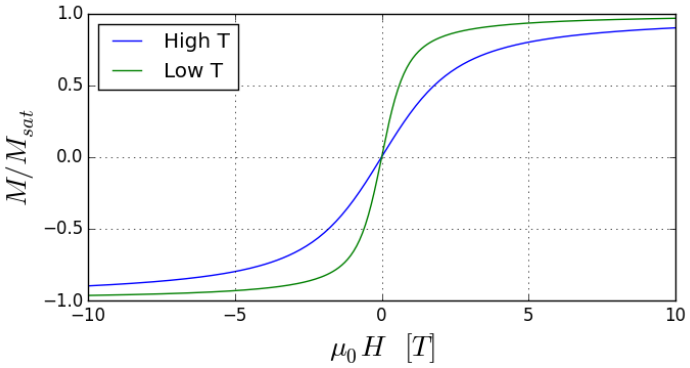


Figure 2.3: Saturation curve of a generic paramagnetic material highlighting the different behavior when the thermal energy is different.

In this way it is generated a magnetization in the material that has the same direction of the applied field and so the material is attracted by the field.
The intensity of this force is well greater than the intensity of the force due to diamagnetism so if a material is composed by atoms that have a non null magnetic moment it behaves as a paramagnetic material, diamagnetism is thus observable just in materials composed by atoms without unpaired electrons.
In these two types of magnetism each atom is assumed to be independent from all the others so the magnetic response depends univocally on the applied field.

The three remaining types of magnetic materials are characterized by the existence of a strong interaction between the magnetic moments of the material called exchange interaction.
The exchange Hamiltonian between two magnetic dipole has the following expression [16]:

$$\hat{H}_{ex} = -J_{ab}(\mathbf{S_a} \cdot \mathbf{S_b}) \tag{2.1.4.1}$$

Where $\mathbf{S_a}$ and $\mathbf{S_b}$ are the spin moments on each magnetic site and $J_{ab}$ is the exchange coupling constant between them. The sign of $J_{ab}$ determines if the lowest energy state is given by parallel or antiparallel alignment of the two adjacent spins giving rise, respectively to ferromagnets or antiferromagnets.
In order to justify the value of the exchange constant we need to understand that this is a purely quantum coupling phenomena that arises from the fact that the atoms with a magnetic moment are always fermions i.e. the total spin is a semi-integer quantity, so the wave function describing their global

state should be antisymmetric.
This statement is crucial because when defining the overall symmetry of a multi-electrons wave function it should be taken into account also the parity of the spin operator.
Since the atomic electron's function strongly depends on the spatial coordinates and the global multi-electron's wave function is obtained by means of a linear combination of the atomic ones the exchange constant is influenced by the overlapping of the electronic functions of two nearest neighbors atoms. This leads to a strong dependence of the sign of $J_e x$ on the lattice parameter in solids.

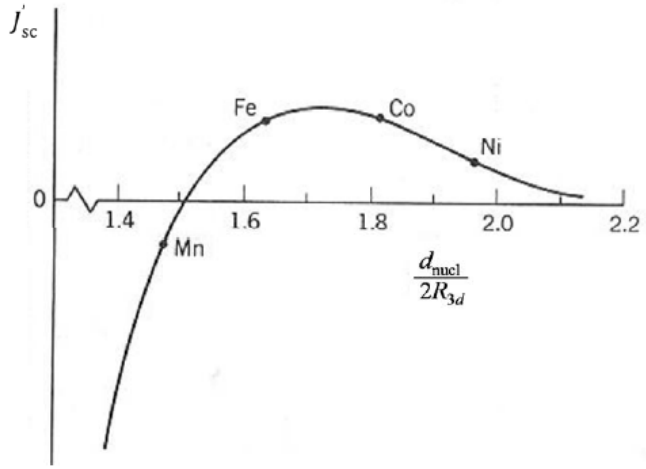


Figure 2.4: Exchange integral evaluated for 3d electrons belonging to nearest neighbors as a function of the ratio between the interatomic distance and 2 times the average spatial extension of the atomic wave function of 3d orbitals. Some significant transition metal are placed on this integral to give some example. Figure from lectures note of prof L. Duó

This is obviously very important from a technological point of view because it introduces the possibility to control the ferromagnetic or antiferromagnetic character of a magnetic material manipulating its lattice parameters.

It can be introduced now the behavior of ferrimagnetic materials, these are materials that present ferromagnetic coupling along a certain direction and antiferromagnetic coupling along another direction. This is clearly induced by a different value of the exchange constant within different plane of

the lattice.
This difference could arises from a physical deformation of the crystal, for example induced by a tetragonal distortion, or from an asymmetry of the electron's wave function of the magnetic atoms. In general it is needed that the exchange constant has a different sign between two different nearest neighbors of the lattice in order to obtain a ferrimagnetic materials.
Obviously also the exchange energy is in competition with the thermal energy so there is a certain temperature at which the exchange energy is comparable with the Boltzmann thermal energy and for temperature above this one the material start to behave like a paramagnet. This temperature is called Curie temperature in the case of ferromagnet and Néel temperature in the case of antiferromagnet [16].

### 2.1.5 Magnetic energy of a body

In the previous section it has been explained how the sign and value of the exchange coupling parameter determines the type of magnetic material that is obtained, in this section we are going to focus on the magnetic configuration of ferromagnetic materials.
Ferromagnetic materials are characterized by a positive sign of the exchange constant between the magnetic sites of the material and due to this fact the magnetic moments are all aligned, this leads to the formation of a macroscopic magnetic moment called magnetization.
The magnetization of a material is a vector quantity, it is defined as the summation of all the magnetic moment present within a certain region of a material, it has the same dimension of the magnetic moment itself and it also has some analogies with it in the way of interacting with a magnetic field.
In order to analyze the magnetic energy of a ferromagnetic material a very common assumption is to consider the magnetization and the field generated by the magnetization itself as two continuous, slowly varying fields. This assumption from a physical point of view means that it is neglected the discrete nature of the distribution of magnetic moments that generates a certain magnetization.
In the framework of micromagnetism this assumption is very useful to predict the orientation of the magnetization of each macro area in which all the spins are assumed to be aligned in the continum limit.
The saturation magnetization ($\mathbf{M}_s$) of a ferromagnet is defined as the magnetization generated when all the dipoles, within a certain macro area, are aligned toward the same direction. It depends mostly on the value of the atomic magnetic moment while, as it will be shown, the equilibrium direction of the magnetization depends on the shape of the material and on its

crystalline structure.
In order to predict what is the magnetization equilibrium direction we have to consider what are all the energy that play a relevant role into its determination.

### Exchange energy

In a solid the exchange energy is obtained as the summation of the exchange energy existing between all the nearest neighbors, a common way to express it is via the Heisenberg Hamiltonian (equaation 2.1.5.1).

$$\hat{H}_{ex} = -\sum_{a<b} J_{ab}\mathbf{S_i a} \cdot \mathbf{S_b} \tag{2.1.5.1}$$

Where $\mathbf{S_a}$ and $\mathbf{S_b}$ are the two magnetic moments on two near sites and $J_{ij}$ is the exchange constant between those two dipole.
In principle in evaluating the total exchange energy within a solid it should be taken into account the interaction between each moment with all the others but since the value of $J_{ab}$ quickly approaches zero as a function of the increasing distance between $\mathbf{S_a}$ and $\mathbf{S_b}$ the energy terms arising from non-nearest neighbor are usually neglected.
In the framework of micromagnetism where the magnetization could be considered as a continuous vector the expression of the exchange energy in a solid can be written in a more meaningful way (see equation 2.1.5.2)

$$E_{ex} = \frac{A}{2}\int_V \left[(\nabla m_x)^2 + (\nabla m_y)^2 + (\nabla m_z)^2\right] dV \tag{2.1.5.2}$$

A is a positive constant called magnetic stiffness and $m_x$, $m_y$ and $m_z$ are the values of the magnetization projected on the three Cartesian axis and normalized on the saturation magnetization.
This expression has an intuitive interpretation considering that a gradient of the magnetization means a tilt between two adjacent spins and thus an exchange energy cost, from this interpretation it can be understand that the greater is A the higher is the energy cost necessary to induce a variation in the direction of the magnetization.
Considering just this argument it seems that a ferromagnet is allowed to show just a uniform magnetization induced by all the spins aligned in what is technically called a "single domain" magnetic configuration.
It is well known that this is not true in reality and in order to explain all the deviation from this behavior we have to take into account other energy therms that play a crucial role.

### Magnetic self-energy

Considering that the divergence of **B** field is always zero and considering that it could be expressed as $\mathbf{B} = \mu_0(\mathbf{H} + \mathbf{M})$ whatever is the material that is considered it holds

$$\nabla \cdot \mathbf{H} = -\nabla \cdot \mathbf{M}$$

This equation has a particularly intuitive meaning across magnetization discontinuity, for example exploiting a surface which contains the edge of a magnetized materials we see that the flux of **M** that is missing outside the material is compensated by the flux of the vector **H**.
This equation thus introduces the existence of a field generated by the magnetization itself indicated with $\mathbf{H}_m$, the sources of this field are all the region in which there is a perpendicular discontinuity of **M**. In a general situation in order to obtain the total **H** field it has to be considered also the field induced by a loop of an external current ($\mathbf{H}_c$).

$$\mathbf{H} = \mathbf{H}_c + \mathbf{H}_m \tag{2.1.5.3}$$

From the relation between the divergences of **H** and **M** it can be understood that the source and sink of $\mathbf{H}_m$ are region in which the magnetization has a sharp change along its direction.
Due to its particular origin it is often used a formal analogy that consists in assuming as sources of the magnetization field the zones in which a magnetic charge density $\sigma_m = \mathbf{M} \cdot \hat{\mathbf{e}}_n$ resides. This field is usually known as the *stray field* outside a magnet or as the *demagnetizing field* within it.
It is now possible to define the magnetic self-energy [17]

$$E_m = -\frac{1}{2}\int_V \mu_0 \mathbf{H}_d \cdot \mathbf{M} dV = \frac{1}{2}\int \mu_0 |\mathbf{H}_d|^2 dV \tag{2.1.5.4}$$

The magnetic self-energy is very important in understanding, at least from a qualitative point of view, the reason for the formation of magnetic domains and the so called shape anisotropy.
The reason for the formation of magnetic domain is, as always in physics, the fact that in some particular condition, a multi domains configuration minimizes the energy of the system. The second expression of the magnetic self-energy (2.1.5.4) implies that the less extended in space is the stray field the smaller is the contribution of the self-energy to the total energy of the system.
Stray field lines can be considered as if they were directed from positive to negative magnetic charge density, thus, in order to minimize the self-energy the most convenient situation is to have adjacent antiparallel domains.This

leads to the existence of adjacent zones with opposite magnetic charge and so a less extended stray field.
This energy is in competition with the exchange energy which is minimized in single domain situation, in which the magnetization is uniform. Depending on the value of the magnetic stiffness A, the dimension and the sample geometry, the material minimize its energy with a different number of magnetic domains separated each other by domain walls which width depends as well on the same parameters.
With similar arguments it is possible to qualitative explain the existence of the shape anisotropy. In order to determine which is the equilibrium direction for the magnetization in a ferromagnet plays a fundamental role the the shape of the material.
According to the fictitious model in which the stray field is generated by magnetic charges it is clear that in order to minimize it, and so the self-energy, it is needed to minimize the magnetic charge density which is directly proportional to the portion of surface transversal to the magnetization. This intuitive argument implies that the magnetization tends to lie parallel to the greater geometrical dimension of the material.
This is very effective in thin film in which the magnetization tends to lie into the plane of the film in order to generate magnetic charges just at the edge of the film, creating thus a very weak stray field in the free space.
Obviously in order to determine which is the most favorable direction for the magnetization to lie also the lattice symmetry plays a fundamental role that will be analyzed in the next paragraph.

### Magnetocrystalline anysotropy

The anisotropy of a magnet can also arises from its crystallographic properties, is well known that the symmetry of a particular lattice strongly influences its magnetic properties.
There are two distinct source of magnetocrystalline anisotropy: single-ion contribution and two-ion contribution.
According to general theory about solids, atomic orbitals are modified when they they belong to a crystal lattice, in particular, depending on the symmetry of the lattice, ionic orbitals can be generated employing different linear combination of the orbitals in free space.
In this process the shape of the electronics cloud around an ion depends on the crystal symmetry and it is going to influence also the magnetic property of the material itself introducing a magnetocrystalline anysotropy.
The two-ion contribution mainly arises from the dipole-dipole interaction Two near magnetic dipole, due to the shape of the magnetic field that each

one generates, minimize their energy in a head-to-tail configuration.
Obviously this interaction has to be averaged on the whole solid, thus, in some particular symmetry, for example the cubic one, the dipole-dipole energy term vanishes. In other crystal in which the cubic cell is stretched the dipole interaction is an appreciable source of ferromagnetic anisotropy.
The combination of this two contributions leads to the definition of a particular crystallographic direction along which the magnetization tends to lie, this crystallographic axis is usually called easy-axis for the magnetization.
The magnetic energy for a material with tetragonal lattice can be expressed as a function of the angle $\theta$ between the easy axis and the direction of the magnetization and the angle $\phi$, defined in the plane perpendicular to the easy axis, as the angle between the magnetization and the less favorable direction for the magnetization in this plane [14].

$$E_a = \int_V \left( k_1 sin^2\theta + k_2 sin^4(\theta)(1 + k_2' cos(4\phi)) + ... \right) dV \tag{2.1.5.5}$$

Considering equation 2.1.5.5 such an energy defines a magnetization that, in absence of external field, tends to point out of plane because is the lower energy direction, but obviously the magnetization can be tilted by external means such as an applied magnetic field.

**Zeeman energy**

It has already been analyzed the energy of a magnetic dipole into a magnetic field, now that the treatment regards macroscopic magnetization the expression is similar but integrated on all the magnetized volume.

$$E_z = -\mu_0 \int_V \mathbf{M} \cdot \mathbf{H} dV \tag{2.1.5.6}$$

This integral is minimized when the magnetization is parallel to the applied field.

All these energy term in a real situation are in competition and the equilibrium position is obtained minimizing the total energy.

$$\begin{aligned} E_{tot} = \int_V \Bigg( & \frac{A}{2} \left[ (\nabla m_x)^2 + (\nabla m_y)^2 + (\nabla m_z)^2 \right] - \frac{1}{2}\mu_0 \mathbf{H}_d \cdot \mathbf{M} \\ & + k_1 sin^2(\theta) + k_2 sin^4(\theta)(1 + k_2' cos(4\phi)) - \mu_0 \mathbf{M} \cdot \mathbf{H} \Bigg) dV \end{aligned} \tag{2.1.5.7}$$

### 2.1.6 Magnetization dynamics and Landau-Lifshitz-Gilbert equation

The knowledge of the energy contributions allows to find the equilibrium position of the magnetization by minimizing the free energy. However, if the magnetization is out of equilibrium, an appropriate equation of motion is needed to describe the dynamics of the system. This requirement is met by the Landau-Lifshitz-Gilbert equation (LLG) that describes the time evolution of a macroscopic magnetic moment in an effective field $\mathbf{H}_{eff}$ [17].

$$\frac{\partial \mathbf{M}}{\partial t} = -\gamma \mathbf{M} \times (\mu_0 \mathbf{H}_{eff}) + \alpha \mathbf{M} \times \frac{\partial \mathbf{M}}{\partial t} = \mathbf{T}_{eff} + \mathbf{T}_{damp} \qquad (2.1.6.1)$$

Here $\gamma$ is the gyromagnetic ratio and $\alpha$ is the damping parameter.
In this equation it has been introduced an effective field $\mathbf{H}_{eff}$ which is representative of all the different energy terms mentioned in the previous section. Since the change in magnetization is always perpendicular to $\mathbf{M}$, the LLG is a torque equation such that any terms on the right-hand side is labeled $\mathbf{T}_i$.
The first term on the right-hand side is called precessional torque, since a miss-alignment of $\mathbf{M}$ and the effective field $\mathbf{H}_{eff}$ leads to a precession of the magnetization around $\mathbf{H}_{eff}$.
The second torque, proposed by Gilbert in 1955 introduces a viscous type damping where $\alpha$ determines the strength of the damping itself. This term is necessary to guarantee a final steady state solution for the dynamics equation in which the direction of the magnetization is stable.
Thus the equilibrium direction for the magnetization is given by the condition $\mathbf{M}_{eq} \times \mathbf{H}_{eff} = 0$ which is true when the magnetization is aligned to the effective field.
From an experimental point of view a material is driven out of its equilibrium configuration changing the overall effective field, this change can be induced, for example, modifying the applied field or stretching the material in order to vary the anisotropy field.
In the last years it has been found that also the injection of a spin polarized current can induce a torque on the magnetization hence a term needs to be added to the LLG equation in order to take into account this effect [18].

$$\frac{\partial \mathbf{M}}{\partial t} = -\gamma \mathbf{M} \times (\mu_0 \mathbf{H}_{eff} + \tau_{FL} \hat{\mathbf{S}}_{FL}) + \alpha \mathbf{M} \times (\frac{\partial \mathbf{M}}{\partial t} - \gamma \tau_{DL} \mathbf{M} \times \hat{\mathbf{S}}_{DL}) \quad (2.1.6.2)$$

Where $\mathbf{S}_{FL}$ and $\mathbf{S}_{DL}$ are unitary vectors giving rise respectively to a field-like torque and a damping-like torque..
The physical meaning of this correction can be understood considering that a polarized current injected into a magnetic material interact, via the itinerant

exchange interaction, with the magnetic dipoles of the lattice, hence its effect is analog to the effect of an additional applied field.
This extra field generates two orthogonal torque $\mathbf{T}_{FL}$ and $\mathbf{T}_{DL}$, the former is always perpendicular to both the vector $\mathbf{S}_{FL}$ and the magnetization, it induces a precession of $\mathbf{M}$ around the field, it is called field-like torque. The second term is always perpendicular to the magnetization and the field-like torque thus it always has the direction of the damping term in equation 2.1.6.1 and due to this fact it is called damping-like term.
It is important to notice that this term has always the same direction of the damping torque in LLG but not the same verse, in fact it could enhance or counteract the damping effect [19].

## 2.2 Transport properties in single layer

Spintronics is the branch of physics that deals with all the phenomena that arise from the modification of band structure of magnetic material induced by the the fact that electrons posses an intrinsic magnetic moment.
The presence of those intrinsic magnetic moments, in a magnetic material, obviously introduces an extra therm in the Hamiltonian describing an electron into such a solid.
Considering for example a ferromagnetic material, being the spin quantization axis parallel to the magnetization, electrons with spin-up or electrons with spin-down, compared to the magnetization direction, posses different energies.

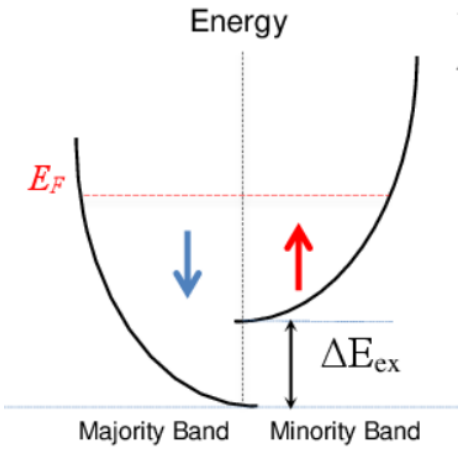


Figure 2.5: Scheme of the splitting of band due to the magnetization.

In the frame work of solid state physics the difference of energy between spin-up and spin-down electrons is translated into a splitting in the energy bands and this implies a spin flip of a number of electrons sufficient to minimize the energy.
If the bands close to the Fermi energy shows a sharp modification the Zeeman splitting can strongly modifies the transport properties of one of the two population of electrons with opposite spin.
Considering also the fact that, due to this energy splitting, also the density of electronic state around the Fermi level varies, we can define a figure of merit used to quantify the difference in the population of spin-up and spin-down electrons called polarization $P_0$.

$$P_0 = \frac{D_\uparrow - D_\downarrow}{D_\uparrow + D_\downarrow} \tag{2.2.0.1}$$

Where $D_\uparrow$ and $D_\downarrow$ represent the density of state at the Fermi level of majority and minority electrons.
The above discussion is intrinsically based on the assumption that the two channels of majority and minority carriers are not exchanging electron each other, i.e. the spin flip event is neglected.
This model is usually referred to as the two-current model in which the spin relaxation time is assumed to be infinite thus the spin flip events are neglected. Obviously this is an over-simplified model but it provides a qualitative and intuitive description of what is the essence of almost all the spintronics phenomena.

It will be shown in this work that spin splitting in conduction band can also be achieved by the existence of a relativistic magnetic field generated in the reference frame of an electron moving into an electric field.
There exist a huge number of spintronics phenomena but since in this work we are dealing with single-layer materials I will mention just those phenomena that concern the magnetic transport properties of single layer.

### 2.2.1 Hall effect

The Hall effect was discovered by Edwin Hall in 1879 [20], it is the most general magnetic transport effect in the sense that it can be observed in the presence of just an electric current and an external magnetic field.
It consists in the generation of a voltage difference across an electrical conductor, transversal to an electric current flowing in the conductor, and to an applied magnetic field perpendicular to the current.

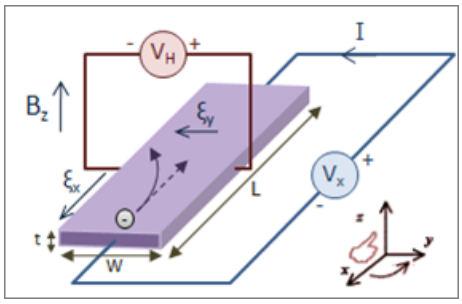


Figure 2.6: Set up used for an hall voltage characterization experiment.

The origin of such a phenomena is directly related to the Lorentz force which is characteristic of any charged particle in motion into a magnetic field. As can be clearly noticed from equation 2.1.1.1 Lorentz force is different from zero if the charged particle has a component of its velocity perpendicular to the magnetic field. The force is always perpendicular to the velocity of the particle, thus if the magnetic field is homogeneous the force induces an orbital motion with a constant radius and with verse determined by the charge of the particle and the relative orientation of the velocity and the field.
Since an electric current is composed by charged particles drifting into an electric field when a perpendicular magnetic field is applied all the electrons, driven by the Lorentz force, are pushed towards one of the two edges of the conductor.

An electric voltage perpendicular to the current direction is the result of this effect.

$$V_H = \frac{I_x B_z}{nte} \tag{2.2.1.1}$$

Where $I_x$ is the current intensity along the **x** direction, $B_z$ is the magnetic field along the **z** direction, n is the carrier density, t is the thickness of the conductor and e is the electronic charge. This phenomena clearly perturbs also the conduction along the **x** direction, the resistivity and hence the conductivity of the material must now be expressed using tensorial relation.

$$\begin{bmatrix} V_x \\ V_y \end{bmatrix} = \begin{bmatrix} R_{xx} & R_{xy} \\ R_{yx} & R_{yy} \end{bmatrix} \begin{bmatrix} I_x \\ I_y \end{bmatrix} \tag{2.2.1.2}$$

If the current is fixed then the longitudinal voltage slightly decreases, because part of the electron flux is deviated towards the transversal direction, this effect is usually called longitudinal magnetoresistance and is even with respect to the applied perpendicular magnetic field.
It is important to notice that , from an experimental point of view, all the parameters that appear into the expression of the Hall voltage, except the carrier density, are usually known, thus the transversal voltage itself could be exploited to estimate the carrier density of a particular electric conductor also if it is not magnetic.

### 2.2.2 Anisotropic magnetoresistance

A current flowing into a magnetic material generates a longitudinal voltage which value depends on the relative orientation between the current itself and the magnetization of the material. The resistivity appears to be higher if the electrical current is flowing parallel to the magnetization and lower if the direction of the current is perpendicular to the magnetization.

$$\rho_{\parallel} > \rho_{\perp} \tag{2.2.2.1}$$

In order to qualitatively understand this anisotropy in the resistivity we have to consider the effect of the spin orbit interaction on the majority electrons channel of a general material. Conduction electrons in a metal, are assumed to posses an s-character, so their conduction properties in principle should not be influenced by the direction of an eventual magnetization of the material since they are spherically symmetric.
The limit of this model arises from the fact that Spin Orbit interaction is actually mixing the spin-up and spin-down states modifying the energy of majority electrons. This effect modifies the energies of d-states raising them

close to the Fermi level of the material. Since we are considering magnetic materials, usually, the d-shell is not completely filled and this introduces the possibility for majority electrons of being scattered into less conductive d-orbitals.
Is important to notice, at this stage, that the above scattering events is effective also at zero Kelvin and does not introduce an extra anisotropy in the resistivity of material but induces just a global increase of the resistance of the majority channel.
However, considering now the effect of a magnetization breaking the crystal symmetry, it can be understood that depending on their orientation, with respect to **M** d-orbitals could be lowered or raised in energy and thus the probability of being occupied or empty changes.
It could be demonstrated using the time independent perturbation theory [21] that the energies of those d-orbitals with lobes perpendicular to the magnetization is lowered while the energies of d-orbitals with lobes parallel to the magnetization direction is raised.
Due to this fact the probability of having a d-hole is higher for d-orbitals with lobes parallel to the magnetization direction, hence a conducting s-electron has an higher probability of being scattered into a d-hole if it is moving parallel to the magnetization, increasing the electrical resistance along this direction.
Another important thing to notice is that the energy difference of d-orbitals depending on their orientation is, obviously, in competition with the Boltzman thermal energy of the electrons, hence, its effect is more effective at low temperature, when $\hbar k_B << \Delta E$. Where $\hbar k_B$ is the thermal energy according to the Boltzman definition and $\Delta E$ is the energy difference between the d-orbitals.

### 2.2.3 Anomalous Hall Effect

Edwin Hall about one year after having discovered the ordinary Hall effect in non magnetic materials observed a similar effect but an order of magnitude greater in magnetic materials [20]. The transversal voltage in the latter case is proportional to the out of plane magnetization instead of being proportional to the external field as it is in non magnetic materials. This effect is called Anomalous Hall Effect (AHE) and its actual physical origin is still a debated scientific topic.

$$V_{AHE} = R_{AHE} I = R_s M_z I \tag{2.2.3.1}$$

As for the ordinary Hall voltage is better to exploit tensor relation in order to obtain a complete description of longitudinal and transversal resistivity.

$$\hat{\rho} \cdot \mathbf{J} = \mathbf{E} \quad ; \quad \mathbf{J} = \hat{\sigma} \cdot \mathbf{E} \tag{2.2.3.2}$$

Where $\mathbf{J}$ is the current density, $\mathbf{E}$ is the electric field, $\hat{\rho}$ is the resistivity tensor and $\hat{\sigma}$ is the conductivity tensor.
Writing explicitly their tensor expressions:

$$\begin{bmatrix} E_x \\ E_y \end{bmatrix} = \begin{bmatrix} \rho_{xx} & \rho_{xy} \\ \rho_{yx} & \rho_{yy} \end{bmatrix} \begin{bmatrix} J_x \\ J_y \end{bmatrix} \quad ; \quad \begin{bmatrix} J_x \\ J_y \end{bmatrix} = \begin{bmatrix} \sigma_{xx} & \sigma_{xy} \\ \sigma_{yx} & \sigma_{yy} \end{bmatrix} \begin{bmatrix} E_x \\ E_y \end{bmatrix} \tag{2.2.3.3}$$

Exploiting some easy symmetry arguments it could be shown that, in an homogeneous material, in which the current is flowing into the plane of the sample $\rho_{xx} = \rho_{yy}$, $\rho_{yx} = -\rho_{xy}$, $\sigma_{xx} = \sigma_{yy}$ and $\sigma_{yx} = -\sigma_{xy}$.
From an experimental point of view we set the current intensity and we record the voltage thus are directly measured the values of $\rho_{xx}$ and $\rho_{xy}$. However, sometimes, it could be more useful to work with conductivity depending on the physical situation and the two are related by:

$$\mathbf{j} = \hat{\sigma} \cdot \mathbf{E} = \hat{\rho}^{-1} \cdot \mathbf{E} = \frac{1}{\rho_{xx}^2 + \rho_{xy}^2} \begin{bmatrix} \rho_{xx} & \rho_{xy} \\ \rho_{yx} & \rho_{yy} \end{bmatrix} \tag{2.2.3.4}$$

Which results into the two relations:

$$\sigma_{xx} = \frac{\rho_{xx}}{\rho_{xx}^2 + \rho_{xy}^2} \quad ; \quad \sigma_{xy} = \frac{\rho_{xy}}{\rho_{xx}^2 + \rho_{xy}^2} \tag{2.2.3.5}$$

And since usually $\rho_{xy}^2 << \rho_{xx}^2$ they are simplified

$$\sigma_{xx} \approx \frac{1}{\rho_{xx}} \quad ; \quad \sigma_{xy} \approx \frac{\rho_{xy}}{\rho_{xx}^2} = \sigma_{xx}^2 \rho_{xy} \tag{2.2.3.6}$$

Despite the origin of the effect is still debated, the scientific community agrees on the fact that there are three main mechanisms contributing to the generation of Anomalous Hall Voltage, two extrinsic and one intrinsic well resumed in [22].
The two extrinsic mechanisms identified by Smit in 1955 [23] and 1958 [24] are known as skew scattering and side jump, both are related to the asymmetric scattering event between a conducting electron and an impurity, depending on the direction of the magnetization. The fundamental difference between the two is that skew scattering can be treated into the approximation of Boltzman traditional transport theory thus just introducing an asymmetric transition probability depending of the relative orientation of $\mathbf{k}$, $\mathbf{k}'$ and $\mathbf{M}$

where $\mathbf{k}$ and $\mathbf{k}'$ respectively represent the electronic wave vector before and after the scattering event while $\mathbf{M}$ is the magnetization vector.
On an other hand the asymmetry arising from side jump event in order to be correctly approached requires a more sophisticated theory in which a scattering event is not just summarized by a transition probability between initial and final state but is investigated also from a microscopical point of view.
It has been accepted by the scientific community that the two extrinsic term give rise to a transversal conductivity which is either linearly proportional to longitudinal conductivity for skew scattering or constant with respect to it in the case of side jump.

$$\sigma_{xy}^{extr} = \alpha_{skew}\sigma_{xx} + \alpha_{sj} \tag{2.2.3.7}$$

Those two mechanisms are, mainly, related to the presence of impurities or defects in a lattice, thus their impact on the macroscopic AHE depends on the quality of the material itself.
This is a fundamental difference with respect to the intrinsic deflection that also is at the origin of AHE. The latter are directly related to a rather complex phenomena based on Berry phase curvature firstly individuated by Karplus and Luttinger in 1954 [25]. Also considering a perfect crystal the presence of a particular lattice symmetry and a non null magnetization, electrons acquire a transversal anomalous drift velocity induced by an extra phase term introduced in the electron wave function by the presence of the magnetization.

$$\sigma_{xy}^{intr} = \alpha_{\phi_B} \tag{2.2.3.8}$$

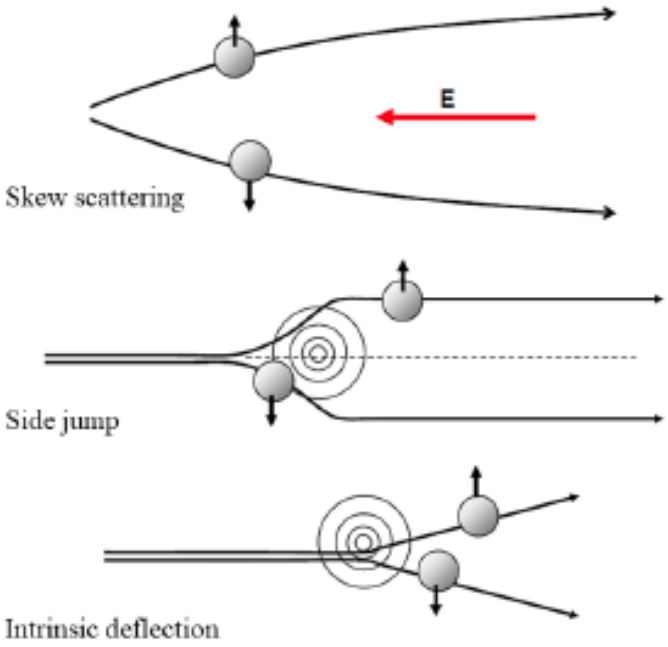


Figure 2.7: Graphical representation of the three different mechanisms that are believed to give rise to Anomalous Hall Effect

Exploiting the above relation between $\hat{\rho}$ and $\hat{\sigma}$ it is possible to obtain similar expression in term of resistivity

$$\rho_{xy}^{AHE} = \alpha_{\phi_B}\rho_{xy}^2 + \alpha_{skew}\rho_{xx} + \alpha_{sj}\rho_{xx}^2 \tag{2.2.3.9}$$

## 2.3 Spin Orbit Torque

Controlling the magnetization of a magnetic material with an electrical current is something of crucial importance in order to integrate new spintronics technologies on the existing electronic devices for example in the memories field [8], [26]. For this reason as soon as Spin Orbit Torque (SOT) was theoretically predicted a lot of experimental and theoretical effort has been devoted to a better understanding of this physical phenomena.
Referring to SOT, usually, people refer to a lot of physical phenomena that have a common origin related, in general, to spin orbit interactions.
In this work, I will consider SOT just in single layer of magnetic material. The essence of this phenomena is the fact that an electrical current, flowing into a material, with a particular lattice symmetry, induces a spin polarization on its own carriers: current induced spin polarization (CISP) [27]. Moreover, if the material is magnetic its atomic magnetic moments are torqued via the itinerant exchange interaction existing between them and the polarized flowing current. It is very important to understand that the peculiarity of this effect is that it is not required an additional layer to provides the polarization, via some interface mediated phenomena, the polarization is induced by the band structure itself which directly depends on the lattice symmetry.
In order to allow the existence of this current induced spin polarization there exist two fundamental requirements: the crystal lattice should lacks of inversion symmetry (locally or globally) and the spin orbit interaction should be not negligible.
Qualitatively we can think that high spin orbit interaction is needed in order to give rise to this effect because it implies that on the reference frame of an electron moving through the electric lattice potential, the relativistic magnetic field strongly interacts with the spin of the electron itself splitting the energy of spin-up and spin-down states. Considering also the relation between this relativistic magnetic field and the electric field produced by the lattice which can be expressed as $\mathbf{B} = -\frac{\mathbf{v}\times\mathbf{E}}{c^2}$ we can qualitatively understand how the lacking of inversion symmetry plays a fundamental role in the generation of CISP. If the electron direction is reverted ($\mathbf{v} \to -\mathbf{v}$) and the electric landscape is non centrosymmetric $\mathbf{E}(\mathbf{r}) \neq \mathbf{E}(-\mathbf{r})$, the relativistic magnetic field felt by electrons wave with opposite k-vector is opposite.

### 2.3.1 k-dependent spin splitting

In order to take into account this effect arising from the combination of high spin orbit interaction and lacking of inversion symmetry in the calculation of

the band structure of a solid an additional Hamiltonian has to be added to the one that takes into account just the kinetic and potential energy.
This work has been done by Rashba and Dresselhaus [28], [29], depending on the symmetry of the lattice the Hamiltonian that takes into account the spin orbit interaction has a different expression.
In this section it will be shown how, from a qualitative point of view, starting from the two different Rashba and Dresselhaus hamiltonians it is obtained a band structure in which spin-up and spin-down electron's state are no more degenerate.
In the following derivation all the constants will be included in $\alpha_R$ and $\gamma_D$ since the aim of the calculation is not to obtain a quantitatively correct model but just to show how from a qualitative point of view CISP arises.
The expression of Rashba and Dresselhaus hamiltonians are [28], [29]:

$$H_{so}^R = \alpha_R(k_y\sigma_x - k_x\sigma_y) = \alpha_R \begin{bmatrix} 0 & k_y + ik_x \\ k_y - ik_x & 0 \end{bmatrix} \tag{2.3.1.1}$$

$$H_{so}^D = -\gamma_D(k_x\sigma_x - k_y\sigma_y) = -\gamma_D \begin{bmatrix} 0 & k_x - ik_y \\ k_x + ik_y & 0 \end{bmatrix} \tag{2.3.1.2}$$

As can be easily calculated, diagonalizing the two Hamiltonian, they have the same eigenvalue (with different constant) so they generate a correction of the free electron dispersion relation with the same symmetry.

$$E_{\pm}^R = \frac{\hbar^2|\mathbf{k}|^2}{2m} \pm \alpha_R|\mathbf{k}| \tag{2.3.1.3}$$

$$E_{\pm}^D = \frac{\hbar^2|\mathbf{k}|^2}{2m} \pm \gamma_D|\mathbf{k}| \tag{2.3.1.4}$$

With eigenvectors:

$$\chi_+^R = \frac{\alpha_R}{\sqrt{2}} \begin{bmatrix} \frac{k_y+ik_x}{|\mathbf{k}|} \\ 1 \end{bmatrix}; \chi_-^R = \frac{\alpha_R}{\sqrt{2}} \begin{bmatrix} \frac{-k_y+ik_x}{|\mathbf{k}|} \\ 1 \end{bmatrix} \tag{2.3.1.5}$$

$$\chi_+^D = \frac{\gamma_D}{\sqrt{2}} \begin{bmatrix} \frac{-k_x+ik_y}{|\mathbf{k}|} \\ 1 \end{bmatrix}; \chi_-^D = \frac{\gamma_D}{\sqrt{2}} \begin{bmatrix} \frac{k_x-ik_y}{|\mathbf{k}|} \\ 1 \end{bmatrix} \tag{2.3.1.6}$$

These give rise to the following expectation values for spin-up and spin-down state.

$$< \chi_+^R|\hat{\sigma}_x|\chi_+^R >= \alpha_R\, sin(\theta_k); \;\; < \chi_+^R|\hat{\sigma}_y|\chi_+^R >= -\alpha_R\, cos(\theta_k) \tag{2.3.1.7}$$

$$< \chi_-^R|\hat{\sigma}_x|\chi_-^R >= -\alpha_R\, sin(\theta_k); \;\; < \chi_-^R|\hat{\sigma}_y|\chi_-^R >= \alpha_R\, cos(\theta_k) \tag{2.3.1.8}$$

$$< \chi_+^D|\hat{\sigma}_x|\chi_+^D >= -\gamma_D\, cos(\theta_k); \quad < \chi_+^D|\hat{\sigma}_y|\chi_+^D >= \gamma_D\, sin(\theta_k) \tag{2.3.1.9}$$

$$< \chi_-^D|\hat{\sigma}_x|\chi_-^D >= \gamma_D\, cos(\theta_k); \quad < \chi_-^D|\hat{\sigma}_y|\chi_-^D >= -\gamma_D\, sin(\theta_k) \tag{2.3.1.10}$$

Where $\theta_k$ is the angle between the k vector and the x direction. And $< \sigma_z >= 0$ for all the possible state.

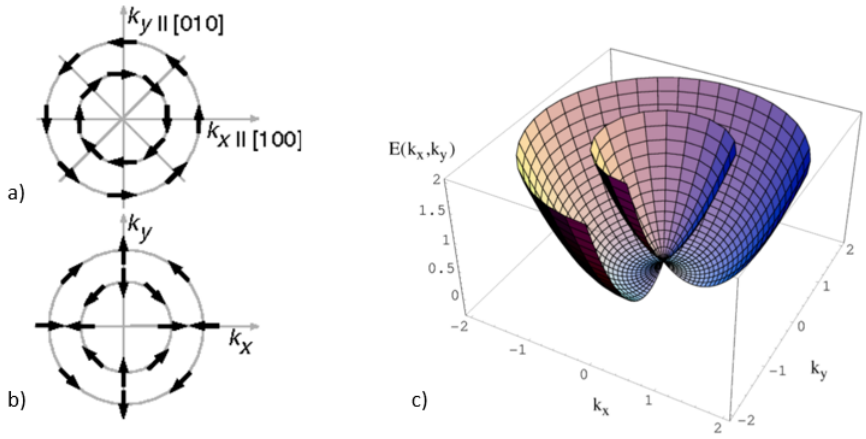


Figure 2.8: In a) and b) is represented the spin texture for the two degenerate Fermi circle respectively for Rashba and Dresselhaaus spin-orbit coupling. The direction of the spin are taken assuming ($\alpha_R > 0$) and ($\gamma_D < 0$). In c) is represented the general dispersion relation due to the k-dependent energy correction of the free-electron energy dispersion relation. According to this dispersion relation $\chi^+$ is the inner branch and $\chi^-$ is the external one. Figure from [30]

As can be seen in figure (2.8) for both the hamiltonians holds the energy relation:

$$E_{n,\chi}(\mathbf{k}) = E_{n,-\chi}(-\mathbf{k}) \tag{2.3.1.11}$$

Depending on the symmetry of the lattice both the Rashba and Dresselhaus Hamiltonian could be present giving rise to particular spin texture and dispersion relation as a function of $\alpha_R$ and $\gamma_D$.
Observing figure 2.8c can be seen that along each possible in-plane k direction there is one spin state with the energy lower than the other one.
However observing figure 2.8a and 2.8b is easy to understand that without an applied voltage the density of electron with a certain k-vector is always equal to the one of the electron with -k and so there is not a net spin polarization in equilibrium situation.

### 2.3.2 Current induced effective field

From an intuitive point of view it can be understood that if a voltage is applied the density of electrons with k-vector anti-parallel to the external electric field direction will be greater than the density of electrons with opposite k-vector. Due to this fact the k-dependent spin polarization is not fully compensated and it arises a net spin polarization which interacts with the lattice through an exchange interaction between itinerant electrons and the magnetic moment of the solid. This effect can also be seen as the torque exerted by a magnetic effective field on the spins of the solid.
We can relate the difference in the population of spin-up and spin-down and thus the absolute value of this effective field to the energy difference between $\chi^+$ ans $\chi^-$ in both the cases of Rashba and Dresselhaus S-O coupling. The whole calculation is well explained in [31], here are reported just the main passages.

$$E(\mathbf{k}, \chi_R^+) - E(\mathbf{k}, \chi_R^-) = g\mu_B |\mathbf{B}_R^{eff}(\mathbf{k})| \tag{2.3.2.1}$$

$$E(\mathbf{k}, \chi_D^+) - E(\mathbf{k}, \chi_D^-) = g\mu_B |\mathbf{B}_D^{eff}(\mathbf{k})| \tag{2.3.2.2}$$

Since for each $\theta_k$ the two spin direction between high energy and low energy state are anti-parallel the effective field lies on this direction and point along the direction of the moment of the lowest energy state.

$$\mathbf{B}_R = \frac{2\alpha_R}{g\mu_B} \begin{pmatrix} k_y \\ -k_x \\ 0 \end{pmatrix} \tag{2.3.2.3}$$

$$\mathbf{B}_D = \frac{2\gamma_D}{g\mu_B} \begin{pmatrix} k_x \\ -k_y \\ 0 \end{pmatrix} \tag{2.3.2.4}$$

The following calculation it will explicitly focus on the effective field arising from Dresselhaus S-O coupling but is easy to obtain similar results in case of Rashba S-O coupling and observing that $\mathbf{B}_R$ and $\mathbf{B}_D$ are orthogonal in case both are present simultaneously the total effective field can be easily obtained summing the two contribution.
When an electric field is applied the Fermi circle is shifted of a quantity $\delta\mathbf{k}$, which is directly proportional to the external electric field $\delta\mathbf{k} = -\mu\mathbf{E}m^*/\hbar$. Where $\mu$ is the electron mobility, $\mathbf{E}$ is the applied electric field, $m^*$ is the effective electron mass and $\hbar$ is the reduced Plank constant. This induces a variation in $\mathbf{B}_D$ which is responsible for the non null net effective magnetic field after averaging on all the involved k-vector.
Since we are, intrinsically, dealing with transport phenomena, just the electron states near the Fermi circle are involved in the generation of the effective

field thus in order to calculate $\mathbf{B}^{eff}$ equation 2.3.2.2 should be evaluated in $\mathbf{k}+\delta\mathbf{k}$ and averaged on a broadened Fermi circle.

$$\mathbf{B}_D^{eff}(\mathbf{k}+\delta\mathbf{k}) = \frac{1}{\pi(k_{F,-}^2 - k_{F,+}^2)} \int_{k_{F,+}}^{k_{F,-}} |\mathbf{k}| d|\mathbf{k}| \int_0^{2\pi} \mathbf{B}_D(\mathbf{k}+\delta\mathbf{k}) d\theta_k \quad (2.3.2.5)$$

Where $\pi(k_{F,-}^2 - k_{F,+}^2)$ is the area of the k-ring which contains all the k-vector that participate to the transport.

$$\mathbf{B}_D^{eff}(\delta\mathbf{k}) = \frac{2\gamma_D}{g\mu_B} \begin{pmatrix} \delta k_x \\ -\delta k_y \\ 0 \end{pmatrix} \quad (2.3.2.6)$$

Considering now the relation between $\delta\mathbf{k}$, the applied electric field and the Ohm law, assuming an homogeneous material we can rewrite it as:

$$\mathbf{B}_D^{eff}(\mathbf{J}) = -\frac{2\gamma_D \mu m^* \sigma}{g\mu_B \hbar} \begin{pmatrix} J_x \\ -J_y \\ 0 \end{pmatrix} = \chi_D \begin{pmatrix} J_x \\ -J_y \\ 0 \end{pmatrix} \quad (2.3.2.7)$$

Where $\mu$ is the electron mobility, $\mu_B$ is the Bohr magneton and $\sigma$ is the conductivity of the material (assumed homogeneous). We have indeed found a relation between the electrical current flowing into the material and the effective magnetic field generated by this current via the spin orbit interaction, the result can be easily extended in the case of presence of both Rashba and Dresselhaus interaction.

$$\mathbf{B}_{D,R}^{eff}(\mathbf{J}) = \chi_D \begin{pmatrix} J_x \\ -J_y \\ 0 \end{pmatrix} + \chi_R \begin{pmatrix} J_y \\ -J_x \\ 0 \end{pmatrix} \quad (2.3.2.8)$$

Looking for a tensor way to express this two relation in order to keep that as general as possible it can be written as:

$$\mathbf{B}_{D,R}^{eff} = \hat{\chi}_D \cdot \mathbf{J} + \hat{\chi}_R \cdot \mathbf{J} \quad (2.3.2.9)$$

And comparing equation 2.3.2.8 with equation 2.3.2.9 we can easily work out a general expression for the two tensor.

$$\hat{\chi}_D = \chi_D \begin{pmatrix} 1 & 0 & 0 \\ 0 & -1 & 0 \\ 0 & 0 & 0 \end{pmatrix} \; ; \; \hat{\chi}_R = \chi_R \begin{pmatrix} 0 & 1 & 0 \\ -1 & 0 & 0 \\ 0 & 0 & 0 \end{pmatrix} \quad (2.3.2.10)$$

It can be observed that this effective field does not depend on the magnetization of the material, but it is clear that if the material is magnetic it

exerts a torque $\mathbf{T}$ on its magnetization $\mathbf{T} = \mathbf{H}^{eff} \times \mathbf{M}$. This torque is usually addressed as field-like torque and it excites a precession of the magnetization around the effective field direction. Obviously, coupled with this effect we have to consider that in the above expression of the torque $\mathbf{M}$ is varying, this is, usually, taken into account introducing another effective field that give rise to the so called damping-like torque. This additional torque term is clearly perpendicular to the field-like term and it can, depending on the symmetry of the lattice, enhance or damp the precession of the magnetization. At this point one can be tempted to derive the corresponding damping-like field computing a cross product between the normalized magnetization and the field-like effective field obtaining

$$\mathbf{H}_{DL}^{eff} = x_{DL}\, \mathbf{H}_{FL}^{eff} \times \mathbf{m} = x_{DL} \begin{pmatrix} J_x \\ -J_y \\ 0 \end{pmatrix} \times \begin{pmatrix} m_x \\ m_y \\ m_z \end{pmatrix} = x_{DL} \begin{pmatrix} -J_y m_z \\ -J_x mz \\ J_x m_y + J_y m_x \end{pmatrix} \tag{2.3.2.11}$$

Which in tensor notation can be written as:

$$\mathbf{H}_{DL}^{eff} = x_{DL} \begin{pmatrix} 0 & -m_z & m_y \\ -m_z & 0 & m_x \\ m_y & m_x & 0 \end{pmatrix} \begin{pmatrix} J_x \\ J_y \\ 0 \end{pmatrix} \tag{2.3.2.12}$$

However the last expression has been obtained considering the magnetization as a simple vector while, instead, what is used is the coefficient representation of a second rank tensor i.e. this coefficients depends on the orientation of the axis. In order to obtain the right expression the procedure is more complicated because it should be take into account the way in which the magnetization vector transform upon the symmetry operations that define the lattice symmetry.

### 2.3.3 Lattice symmetry and spin orbit torque

A crystalline solid is a solid material whose constituents such as atoms, molecules, or ions are arranged in a highly ordered microscopic structure, forming a crystal lattice that extends in all directions. Being the constituents ordered every crystalline lattice posses a particular symmetry, and this symmetry drastically influences the physical macroscopic properties of the solid. The set of symmetry operation that leave a central crystallographic point fixed while moving the edges and faces of the crystal to the positions of features of the same size and shape defines the point group of a certain crystal. Since the symmetry of the lattice is possessed also by the electric potential that characterize the Hamiltonian of the problem is clear that this symmetry

will strongly influence the electronic and optical properties of the solid.
Neumann's principle formalize this statement: any types of symmetry which is exhibited by the point group of the crystal is possessed by every physical property of the crystal, also considered at a macroscopic level.
This principle clarify the fact that if we want to know what is the correct expression of current induced SOT field we have to deal with the symmetry point group of the crystal, exploiting it, in the proper way, it will be possible to obtain the general tensor associates to any particular macroscopic physical property.
The right way of calculating those tensors is well explained in the book "Symmetry and Magnetism" by R. R. Biress [32]. Here I present the summary of fundamental steps for the calculation of the field-like and damping-like fields for the particular lattice symmetry of the material that has been used for this experimental work.
The first clarification that has to be done regards the fact that current and magnetization are not simply vectors because their expression is not invariant whit respect to the choice of the axis orientation. We start from the fundamental assumption that the current induced spin polarization $\mathbf{S}$ is linearly proportional to the current density $\mathbf{J}$ and they are connected by a second rank tensor $\hat{\eta}(\mathbf{m})$ which is a generic function of the normalized magnetization $\mathbf{m}$.

$$\mathbf{S} = \hat{\eta}(\mathbf{m}) \cdot \mathbf{J}$$

Proceeding with the Einstein notation and assuming that $\hat{\eta}(\mathbf{m})$ can be expanded is power of the magnetization it is obtained

$$S_i = \eta_{ij} J_j = (\eta_{ij} + \eta_{kij} m_k + \eta_{lkij} m_k m_l + ...) J_j$$

Being $\mathbf{S}$ a spin polarization, from a symmetry point of view it behave exactly like a magnetic moment, thus it is odd upon mirror reflection symmetry operation i.e. $\hat{R}_s(\mathbf{S}) = -\mathbf{S}$ and it is odd also upon time inversion symmetry $\hat{I}_t(\mathbf{S}) = -\mathbf{S}$. Where $\hat{R}_s$ and $\hat{I}_t$ represent here respectively space and time inversion symmetry operators.
In the next table it is reported the notation used where $R_s$ and $I_t$ respectively represent the eigenvalues of space mirror reflection and time inversion symmetry operators.

| Notation | $R_s$ | $I_t$ |
|---|---|---|
| i-polar | 1 | 1 |
| i-axial | -1 | 1 |
| c-polar | 1 | -1 |
| c-axial | -1 | -1 |

Table 2.1

The eigenvalues of the inversion operators have an important role in calculating what is the symmetry of a third mathematics object resulting from the multiplication of two others with a defined symmetry. The symmetry of the product of two generic tensor is given by the multiplication of the eigenvalues of the symmetry operator applied to the two original tensors.
Using the notation of 2.1 , **S** is a c-axial tensor also all the terms that appears in its expansion must have this symmetry, exploiting this fact and the multiplication rules mentioned above we can understand what is the symmetry needed for $\eta_{ij}$ and $\eta_{kij}$. Looking at the zeroth order term, since $J_j$ is c-polar tensor, $\eta_{ij}$ must be i-axial. Considering the second order term in which also the magnetization (c-axial) appears in order to respect the symmetry of **S** $\eta_{kij}$ is needed to be i-polar.
A direct consequence of Neumann's principle is that once we know what should be the symmetry properties of a tensor in term of space reflection and time inversion symmetry operation we can obtain what is the most general expression of this tensor with respect to the point group symmetry possessed by the crystal.
The crystalline point group symmetry of the material that has been used for this experimental work is $\bar{4}2n$ and exploiting the table 4 and 7 of [32] we find what is the tensor expression of $\eta_{ij}$ and $\eta kij$.

$$\hat{\eta}(\mathbf{m}) = \eta^{(0)} \begin{pmatrix} 0 & 1 & 0 \\ -1 & 0 & 0 \\ 0 & 0 & 0 \end{pmatrix} + \eta^{(1)} \begin{pmatrix} 0 & am_z & cm_y \\ am_z & 0 & bm_x \\ cm_y & bm_x & 0 \end{pmatrix} \qquad (2.3.3.1)$$

Where $\eta^{(0)}$ and $\eta^{(1)}$ are constant.
The two obtained tensors directly relates the current flow to the generation of an effective field that torques the magnetization of the material, this method is very general and allow us to understand just observing the point group of a particular crystal if it will generates current induced spin polarization. Moreover the two obtained tensors perfectly match with the tensors calculated with different theoretical argument in [11].
This argument gives us just an information about the direction of the spin

polarization but not about the values of $\eta^{(0)}$ and $\eta^{(1)}$, the physical origin of the value of this two parameter is still under debate in the scientific community.

## 2.4 Overview on half-metallic compensated ferrimagnet

In 1995, new class of magnetic material was proposed by van Leuken and de Groot in [33], which they called a half-metallic antiferromagnet.
They proposed a theoretical study regarding the magnetic and electric properties of this new class of material particularly interesting for spintronics application.
According to their prediction this new materials, from a magneto-transport point of view, should behave similarly to an half metal i.e. the Fermi level was predicted to be in the middle of a band gap for the minority electrons while in a conducting band for the majority carriers.

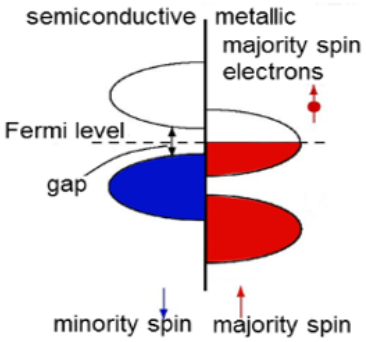


Figure 2.9: Schematic representation of the band structure of an half-metal.

In figure 2.9 it could be understood why for this kind of materials it is expected a theoretical spin polarization, defined as in equation 2.2.0.1, of 100%.
According to Leukan and de Groot prediction, the peculiarity of 'half-metallic antiferromagnet' is the fact that while being equivalent to an half metal from a band structure point of view they would be also equivalent to an antiferromagnet from a magnetic point of view with a low magnetic net moment and thus small stray field and fast dynamics.
The combination of those two predicted properties makes this kind of material very interesting for spintronics application and general research because they would combine some of the most interesting properties of antiferromagnets, such as scalability and stability, while providing a spin polarization comparable with the one obtained using conventional ferromagnets.
Because of this reason, since this research was published a lot of experimental effort has been spent to the fabrication of such a material and eventually

it was produced as $Mn_2Ru_xGa$ (MRG) for the first time by Kurt in 2014 [10]. MRG has two equal, oppositely orientated but crystallographically-inequivalent, magnetic sublattices. The crystal has an inverted $L2_1$ structure as shown in Figure 2.10.

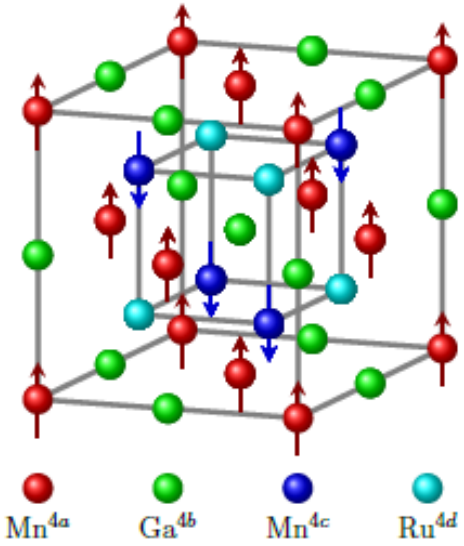


Figure 2.10: Crystallographic representation of the $L2_1$ structure.

The Mn atoms at the 4a and 4c sites are responsible for the magnetism of the material. Since 4a and 4c are crystallographically-inequivalent the moments of each sublattice have different temperature dependence, with the Mn-4a moment remaining roughly constant as a function of temperature and the Mn-4c moment decreasing with increasing temperature (See Figure 2.11). Being the two antiferromagnetically coupled this allows for compensation of the net moment at a temperature $T_{comp}$ where the moments are equal in magnitude, but opposite in direction [34].

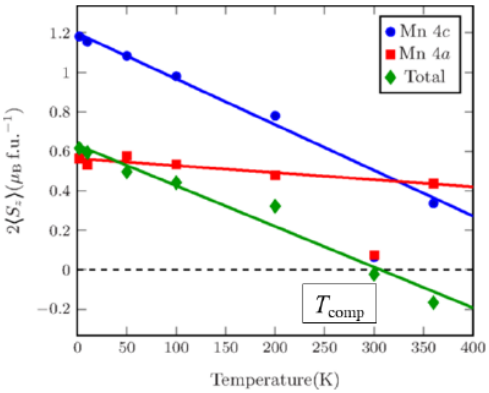


Figure 2.11: Temperature dependence of the magnetization of 4c and 4a lattice.

The compensation temperature can be tuned by changing the concentration of Ru, where lower Ru concentration causes a lower $T_{comp}$, but also by substrate induced strain. The Ru concentration also tunes the position of Fermi level so as to position it into the spin gap.

Being crystallographically-inequivalent the two Mn sublattices posses different electronic structure, in particular 4c has a metallic character while 4a presents an energy gap around the Fermi level behaving similarly to a semiconductor.
Due to this fact, in first approximation, just 4c sublattice participates to electronic transport phenomena i.e. conducting electrons interact just with Mn-4c and thus with a ferromagnetic lattice.
In figure 2.12 it could be noticed that if a magnetic field is applied the net magnetization is aligned toward the direction of the field but the orientation of Mn-4c moment changes.
This has a strong impact on transport measurement because since the current interacts just with 4c lattice we track just its magnetization, meaning that anomalous hall signal has opposite sign above or below compensation.

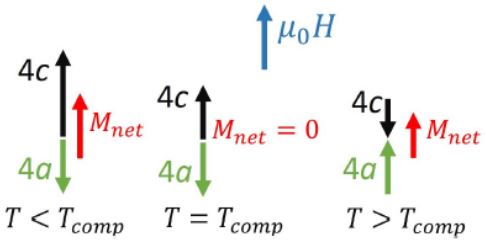


Figure 2.12: Schematic representation of the orientation of Mn-4a, Mn-4c and net moment with a constant applied field and temperature above or below compensation.

The fact that an electrical current just interacts with 4c sublattice induce a polarization of the current which, theoretically, in absence of Spin Orbit interaction and at zero kelvin should be 100%.
Although since SOI modifies the energy of the d-states in the minority band it appears that, also at zero kelvin, some of them populate the energy gap and thus participate to electronic transport, moreover also the effect of a finite temperature obviously decreases the spin polarization of the electric current.
An experimental value that has been measured [35] for the polarization (as defined in Equation 2.2.0.1) is 58%. Such value is comparable with the polarization that could be achieved exploiting an ordinary ferromagnet but the in the case of MRG the stray field is negligible and the dynamics of the magnetization is faster.

# Chapter 3

# Experimental methods and sample characterization

The experimental work that concerns this thesis has been done using thin films of $Mn_2Ru_xGa$. The films were grown by magnetron sputtering in the Shamrock sputtering cluster on a substrate of MgO. The choice of the substrate is particularly important because it, obviously, induces a strain in the crystal of MRG and thus it strongly influences its magnetic properties. In particular the in-plane lattice parameter of MgO along the [100] direction almost perfectly matches with in-plane lattice parameter of MRG along the [110]. The small mismatch that exists between the above cited lattice constants is very important to determine the magnetic anisotropy of the thin film.
Being a thin film, according to the effect of shape anisotropy the easy axis for the magnetization should lie in the plane of the film, however the small mismatch between the two lattice parameters induces a slight tetragonal distortion to the perfectly cubic crystal. This distortion has the effect of changing the easy-axis for the magnetization from in-plane to out-of-plane.
After the fabrication crystallographic characterization was performed by means of X-ray techniques in order to verify that the lattice properties were correctly obtained.
Magneto-transport characterization was performed exploiting Anomalous Hall signal recorded with lock-in amplifier and using an AC current generator at 517 Hz, in order to control the magnetization three different instruments have been used, able to perform also measurement varying the temperature.

- 4 T supermagnet with helium-flow cryostat
- 14 T supermagnet with helium-flow cryostat and rotating field (ppms)

- 2 T multimag with rotating field

## 3.1 Sample fabrication and structure characterization

The samples used for this experimental work are thin films of $Mn_2Ru_xGa$ grown on a substrate of MgO by means of DC magnetron sputtering, the thickness is 20 nm and it is all coated with an oxide layer which has the role of preventing the material from oxidation which would damage the magnetic state of the film.
I thank Dr. Gwenael Atcheson who grew the sample and helped me with their characterization.

### 3.1.1 DC magnetro sputtering

DC magnetron sputtering is a physical vapor deposition technique used for epitaxial growth of thin film of various material. The basic mechanism consists in exploiting a plasma in order to sputter ions from a certain target and then deposit the sputtered ions on a particular substrate, via diffusion or drift mechanism.
In order to control the collision between ions of plasma and target a DC electric potential is applied between anode (substrate) and cathode (target) to accelerate plasma's ions towards the cathode. A common noble gas that is used to ignite and sustain the plasma is Argon, it maintained at a pressure between 1 and 100 mTorr.
In figure 3.1 it is shown a typical scheme for a magnetron sputtering set-up.

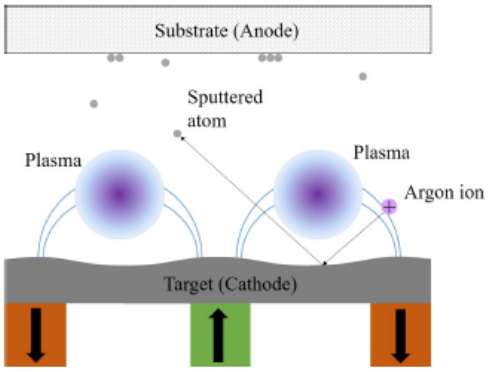


Figure 3.1: Mgnetro sputtering typical set up.

Observing figure 3.1 it is be seen what is the role of the permanents magnets that are placed underneath the target. They are employed to confine the plasma in a region close to the target in order to enhance the ablation process and, secondly, also to trap the plasma's electrons from being accelerated towards the substrate in order to prevent it from heating.
To obtain epitaxial growth of $Mn_2Ru_xGa$ (MRG) an MgO [001] substrate is used, Ru and $Mn_2Ga$ are co-sputtered from two confocal magnetron gun.
As explained in section 2.4 the Ruthenium concentration tunes the compensation temperature of MRG, when x=0.5 (in $Mn_2Ru_xGa$) $T_{comp}$ is at room temperature otherwise it could be shifted changing Ruthenium concentration.
From an experimental point of view Ruthenium concentration is tuned by varying the sputtering power of the $MN_2Ga$ gun, while the power of the Ru gun is maintained constant.
As explained above, experimentally, is important to fabricate samples that have an effective out of plane anisotropy, otherwise the AHE (See paragraph 2.2.3) signal would not give us any useful information on the magnetization. This out of plane anisotropy is achieved thanks to the slight mismatch between MRG [001] and MgO [011] which is responsible of the tetragonal distortion and thus of the out of plane anisotropy.
This clearly limits the thickness which is possible to achieve preserving the tetragonal distortion of the crystal because increasing the thickness the film tents naturally to relax to a cubic structure. The experimental limits that has to be respected in order to obtain out of plane anisotropy is about 50 nm.

### 3.1.2 X-ray structure analysis

The first characterization that has to be done deals with the structure analysis which allows us to understand if the fabrication process ended properly and the crystal has the expected symmetry.
X-ray are widely used in solid state physics in order to characterize crystalline lattice because of their wave length which is comparable with the inter-atomic distance in most of the solids of interest.
In particular, it was performed on the sample employed for the experimental work of this thesis XRD (X-ray diffraction) to derive the out of plane lattice constant, RSM (reciprocal space map) to explore the in plane lattice parameters and XRR (X-ray reflection), to determine the thickness of the layers and the quality of their interfaces. All those techniques exploit the fact that light, being a wave, suffers of diffraction and interference, so it is able to give us a lot of information about the lattice of a material. Two waves propagating in

the same region of space can interact constructively or destructively depending on the phase difference between them. When two waves are diffracted by two different planes of a lattice, depending on the distance between the two planes, it is observed a different results. A schematic representation of this process is represented in figure 3.2.

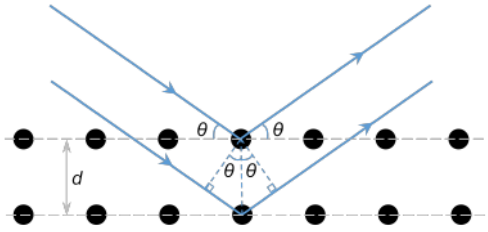


Figure 3.2: A wave impinging on the surface of a sample is reflected by every lattice plane until it vanishes, depending on the distance between lattice planes, there is just a particular set of $\theta$ that gives rise to reflection picks.

The condition necessary to obtain constructive interference is described by the Bragg's law and gives us an information about the d-parameter which in this case represents the distance between two different lattice planes.

$$2d\sin(\theta) = n\lambda \tag{3.1.2.1}$$

Where $\theta$ is the angle between the incident wave and the film surface, $\lambda$ is the wave length and n is an integer and positive number (n $\in$ N).
It is very important to understand that in a crystalline lattice each planes can, at the right angle, satisfy the Bragg's condition, not just the planes that are parallel to the surface. This results in the fact that, impinging with a single $\mathbf{k}_{in}$, a certain number of $\mathbf{k}_{out}$ are obtained.
All the x-ray characterization were performed exploiting two different instruments shown in figure 3.3.

Figure 3.3

### XRD characterization

X-ray diffraction characterization was performed using "Philips PANalytical X'Pert XRD system". With this instrument it is possible to obtain information concerning the out of plane (c) parameter of the lattice. Obviously the most intense pick is the one produced by the out of plane lattice constant of MgO which is more intense because of the huge difference in terms of thickness between substrate and film.

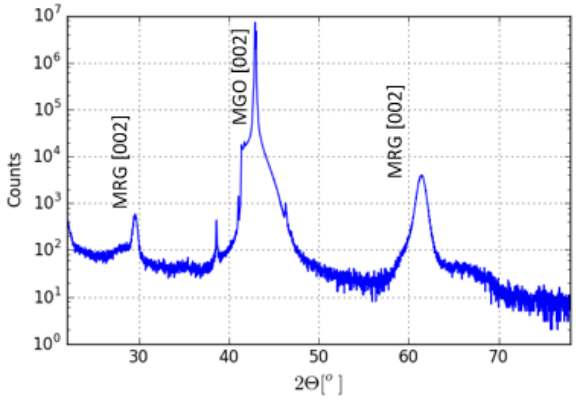


Figure 3.4: XRD spectra of one of the sample of MRG used during this work.

From the position of the peaks it is possible to extrapolate the out of

plane lattice parameter, using the Bragg's law and knowing the wave length of the incident beam. In figure 3.4 it is possible to obtain the $\theta$ corresponding to [002] lattice plane of MRG and thus the c-lattice parameter which is 603 pm in the studied sample.

### RSM characterization

Reciprocal space map is carried out using the "Bruker D8 Discover diffractometer". This instrument, also, is based on X-ray diffraction but allows to obtain information also regarding the in plane arrangement of the crystal, in particular it is possible to evaluate the in plane (a) lattice parameter of the crystal.

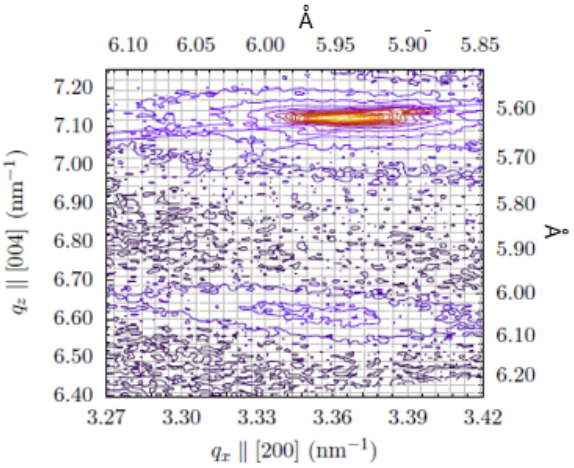


Figure 3.5: Reciprocal space map.

From figure 3.5 it can be estimated the a-lattice parameter which in this case is 596 pm. Combining this results with the one obtained in the previous paragraph it is possible to quantify the tetragonal distortion as $(c - a)/c$ which in this case is 1%.
This confirms that, at least from a structural point of view, the film was produced in the proper way.

### XRR characterization

This technique exploits in a slightly different way x-rays, instead of looking to their diffraction pattern a reflectivity analysis is performed. As it is well

known from geometrical optics when there is an interface between two optical media characterized by different refraction index there exists a critical incidence angle beyond which light is completely reflected.
This effect is exploited to estimate the density, the interface roughness and the thickness of a layer or multi-layer structure.

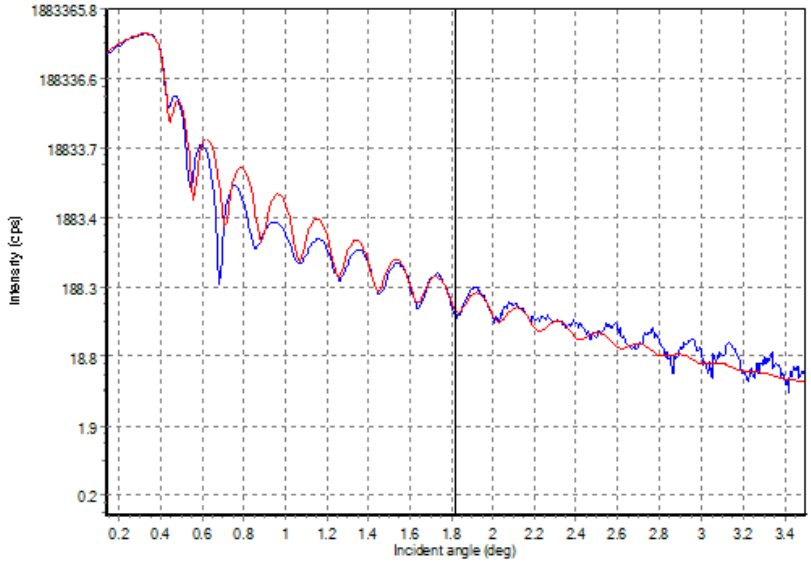


Figure 3.6: XRR scan of GAC325. In red the fitting, in blue the measurement.

The thickness is estimated from the interference between x-rays reflected from the first interface (air-MRG) and x-rays reflected from the second interface (MRG-MgO). As a function of $\theta$ we can observe, in figure 3.6, maxima and minima of the reflected photon's number, this oscillating behavior is consistent with equation 3.1.2.1, moreover, we can obtain an information about the roughness of the interface looking to the angle at which those oscillation becomes too noisy.
The density is derived from the total reflectivity at low angle, which clearly depends on the density of the material.
Those estimation are done by a software that takes as an input the layer structure and all the information known about the materials and then fits the counts profile estimates thickness, density and roughness of the interfaces.
From the fitting and measurement shown in figure 3.6 it has been estimated a thickness of the MRG later of 20 nm, a thickness of the TiN tapping layer

(to prevent from oxidation) of 3 nm and a quite rough interface between those two.

### 3.1.3 Patterning

After the fabrication it is obtained a blanket thin film of the desired material, in order to perform precise electric characterization it is usually patterned in an hall bar configuration.
The pattern allow us to measure separately the longitudinal voltage: $V_{xx}$ and the transversal Anomalous Hall Voltage: $V_{xy}$ (view equation 2.2.3.1).

The patterning process of the hall bar is done in two different steps:

- UV-Lithography
- Ion Milling

Those steps depending on the final goal of the process might be repeated several times. During my thesis I participated to all the patterning process of several hall bars, starting from the blanket film ending up with the final device. The Uv-Lithography was performed in the class 100 cleanroom of CRANN laboratory using the OAI Ultraviolet Mask Aligner shown in figure 3.7a while the ion milling was performed using the Millatron in the cleanroom of SNIAM shown in figure 3.7b.

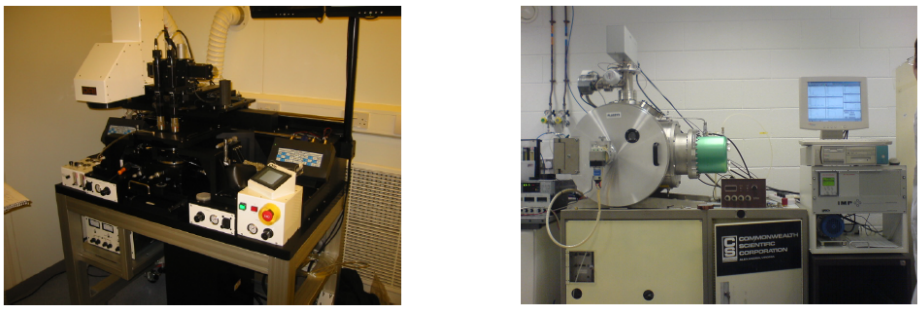

(a) (b)

Figure 3.7: UV-mask aligner (a) and Millatron (b)

### UV-Lithography

Uv-Lithography is a process that exploits UV light in order to transfer a certain micro-metric geometry from a mask to a sample. The first step consists in coating the blanket film of interest with a layer of photoresist exploiting a spincoater, it is possible to tune the thickness of the coating layer changing the rotational speed of the spincoater.
The coating layer is made of a polymer which properties are strongly modified by interaction with UV-light, depending on the final device that has to be fabricated, it can be used a positive photoresist which hardens when exposed to UV-light or either a negative photoresist which weakens when exposed to UV-light.
Before exposing it to light the coated sample is pre-baked for two or three minutes and then transferred to the mask aligner, after having fixed the position of the mask the photoresist is exposed to UV-light for few second.
The next step consists in exploiting a particular solvent, called developer, in order to remove photoresist from the designed regions, those, depending on the photoresist used, could be the exposed regions or the others.
At this point the sample is ready to be etched.

### Ion Milling

After having patterned the coating layer, the pattern itself has to be transferred to the film, a common way of doing it is exploiting an ion milling process. This step is performed in the SNIAM cleanroom using the Millatron machine.
The sample is placed on a rotational stage in a vacuum chamber operating at a base pressure of $5 \times 10^{-7}$ Torr. A thick layer of positive photoresist protects the regions of the film underneath it from the ion beam. All of the other regions of the sample are etched away. The photoresist layer is thicker than the sample so even if the photoresist is etched faster than the sample, there is always a thin layer of resist left after the etching process to protect the film underneath it. The Millatron operates by creating highly energetic ions of argon gas, which are then accelerated towards the sample. The argon working pressure is $7 \times 10^{-7}$ Torr and its flow is controlled by a manual needle valve. The $Ar^+$ ions bombard the film and eject atoms from the surface of the sample. It is important to know when to stop the etching, and for this purpose there is a secondary ion mass spectrometer (SIMS) located on top of the vacuum chamber. The sample is positioned at a certain angle with respect to the beam, and the atoms ejected from the surface become ionized and some of them travels to the SIMS detector. By monitoring the

atomic mass of the detected ions the etching process can be controlled. It is a very directional method of etching, compared with chemical wet etching, and hence does not produce a strong wedge effect.

### Hall bar patterning process

In order to obtain as a final result an hall bar device the first step is to pattern the hall bar shape, this is done using negative photoreist in order to coat all the layer, then, exploiting a particular mask, UV-rays are focused just on the designed shape of the hall bar, hardening that region.
After this process the developer is used to remove all the photoresist that does not protect the designed device. The next step consists in etching all the MRG that surrounds the hall bar, this is done in the Millatron machine in which the whole film is bombarded by ions until the substrate is reached, since the hall bar is covered by the photoresist it is not damaged.
At this point it is necessary to pattern the contacts, it is done exploiting UV-lithography, this time using positive photoresist. UV-light is focused just on the designed contact, making that region of coating layer weaker. The film is than developed in order to remove the photoresist from the contacts while all the other regions are protected. Titanium atoms are then deposited on all the sample and then covered by gold (titanium is used because gold directly on MgO is not very durable). Now it is possible to clean everything with acetone in order to remove all the photoresist in excess. A picture taken with an optical microscopy is shown in figure 3.8 of the obtained hall bar after all the above process.

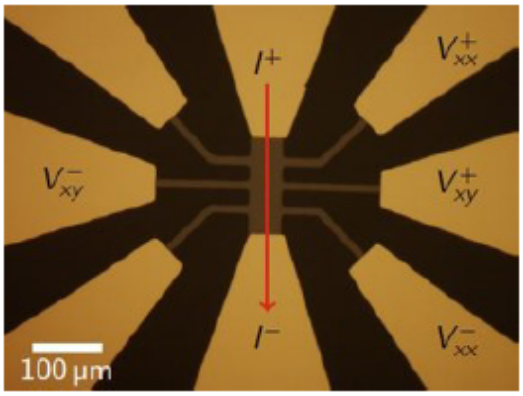


Figure 3.8: Optical microscope picture of a typical hall bar patterning.

## 3.2 Magnetic properties characterization

In order to characterize Spin Orbit Torques effect which is the final aim of this work it is necessary to characterize the sample from a magnetic point view to then obtain some quantitative estimation of SOT parameters.
As already pointed Anomalous Hall Effect is exploited to track the magnetization projection along the z-axis (out of plane).

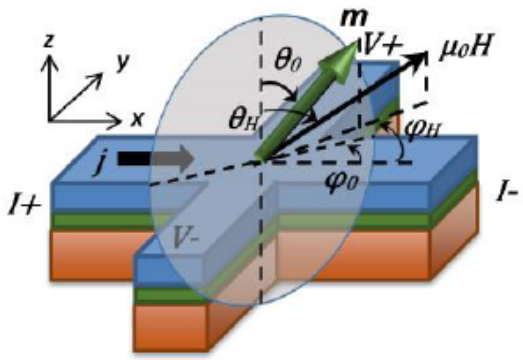


Figure 3.9: Sketch of the experimental set-up. The external field, for the majority of the experiments that we did was either in the plane of the sample or out of plane.

All the measurement were performed using an AC current with a frequency of 517 Hz, the importance of exploiting an AC signal is that it allows us to perform analysis of second and third harmonics that, as it will be explained later, contain important information about SOT effect. However the time that an antiferromagnet takes to reaches a new equilibrium after a perturbation is very short, it results in a frequency which is well greater than 517 Hz, thus, during all the analysis it was possible to use a quasi-static approximation.
As current source it was used a Keithley which can provide a current at different frequency and different intensity. In order to record the signals lock-in amplifiers (Zurich instruments) were used to maximize the signal to noise ratio, which is crucial especially when the goal is to record higher harmonics that for obvious reason possess a very small signal.

### 3.2.1 Principle of lock in amplifier detection

Lock-in detection is a very powerful technique that exploits as a basic principle the fact that modulating and demodulating signal at a certain frequency allows to filter, together with the signal, also the white noise that, depending on how narrow is the filter in term of frequency, can be drastically reduced. Another very important feature is that the demodulation frequency can be chosen so that it is possible to record also signal on second and third harmonics if they are needed.

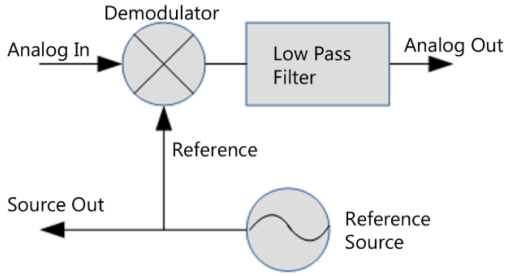


Figure 3.10: Simplified scheme of lock-in modulation and demodulation technique.

In figure 3.10 it is possible to have a qualitative idea of how a lock-in amplifier works, the signal that has to be measured is multiplied times an oscillating reference signal, which frequency can be externally chosen. The resulting signal passes through a low pass filter which cut-frequency is chosen in order to limit as much as possible the noise, the signal is than demodulated to obtain the original input.
In all the measurement that I performed during the thesis the frequency of the reference signal was always set to be equal to the frequency of the AC current exploited, this makes easier to, lately, perform harmonics analysis.

### 3.2.2 Determination of compensation temperature

As it was explained in the section regarding the properties of $Mn_2Ru_xGa$, depending on the amount of Ruthenium that was used the temperature at which the magnetization of the two different sublattices is equal and opposite, varies.
The first measurement that has to be done is, to record $V_{xy}$ Signal as a function of temperature in a constant, out of plane, field.

The obtained measurement is shown in figure 3.11.

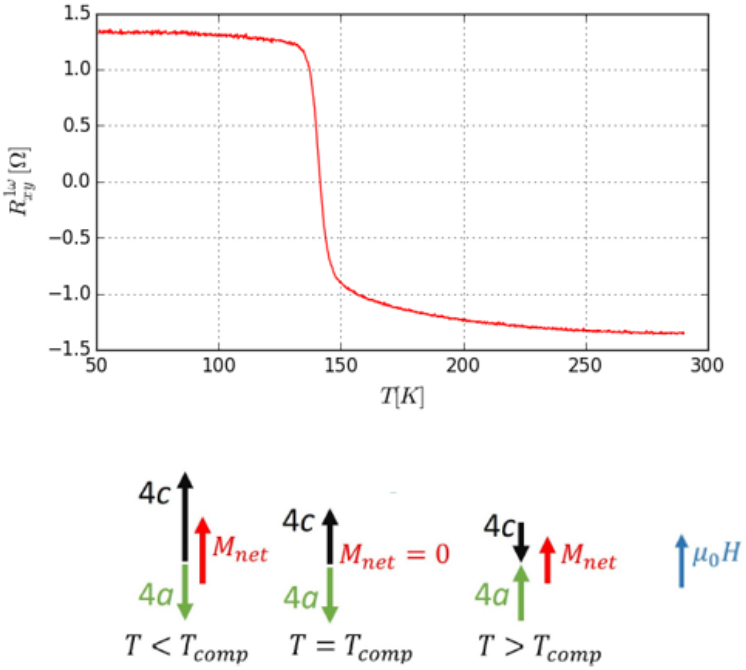


Figure 3.11: The figure represents the value of $V_{xy}^{1\omega}$ normalized in current while the temperature increase from 10 K to 290 K at a slow rate of 1 K/min. In the bottom figure it could be seen a schematic representation of how the two different sublattices are behaving in term of orientation and amplitude of the magnetic moments as a function of temperature.

The compensation temperature can be deduced from this plot, when the signal quickly changes it means that the Mn-4c has switched and this is due to the fact that the magnitude of its moment became smaller than the magnitude of the magnetic moment of Mn-4a.
The estimated compensation temperature from this measurement is about 145 K, in next section this temperature will be confirmed also by different experiments.

### 3.2.3 Determination of coercive field and ordinary Hall effect

In order to characterize, from a magnetic point of view, a certain material, it is very important to understand how it behaves as a function of the applied

magnetic field. In general, depending on the application, it is better to have magnetic materials highly sensitive to external magnetic field, for example in case of field sensors. In other application, are preferred materials that are very robust against magnetic field, as in the case of memories, in which an information is encoded with the direction of the magnetization.
As it was explained in section 2.1.5 there are several physical reason that determines which is the easy-axis for the magnetization in a magnetic material. Exploiting the slight difference between the lattice constant of MgO and MRG it has been engineered the easy-axis to be out of plane, thus, applying an out of plane field from -4 T to 4 T, we expect to obtain the typical hysteresis loop. The results is shown in figure 3.12 for all the different temperature measured.

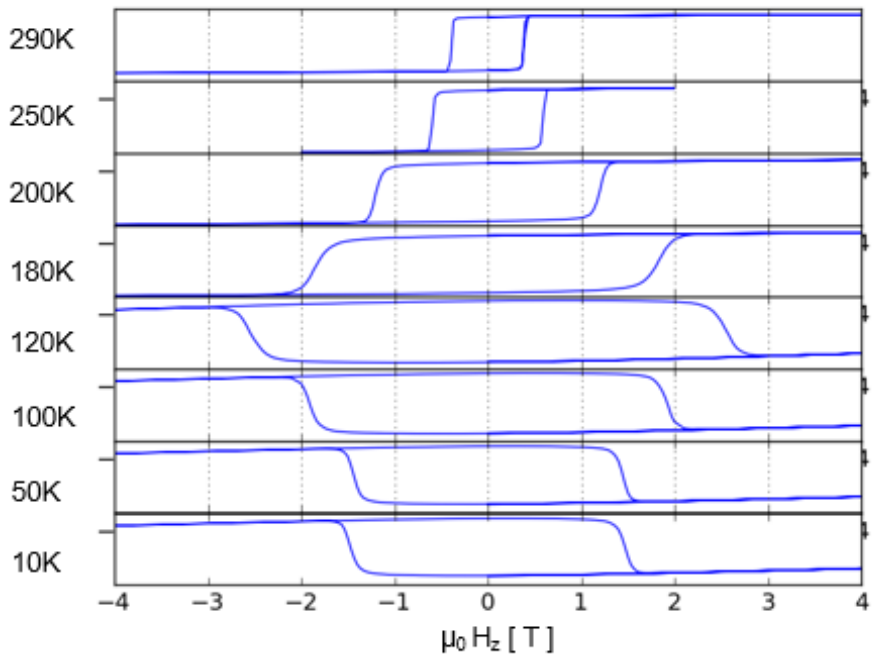


Figure 3.12: Out of plane field loop performed at a set of different temperature. It can be seen that between 120 K and 180 K the compensation temperature is crossed.

Defining the coercive field as the field that is necessary to switch the magnetization from $-m_z$ to $+m_z$, where the z-axis points out of the sample plane, we can see in figure 3.13 that it clearly diverge approaching the compensation temperature at 140 K, from both side.

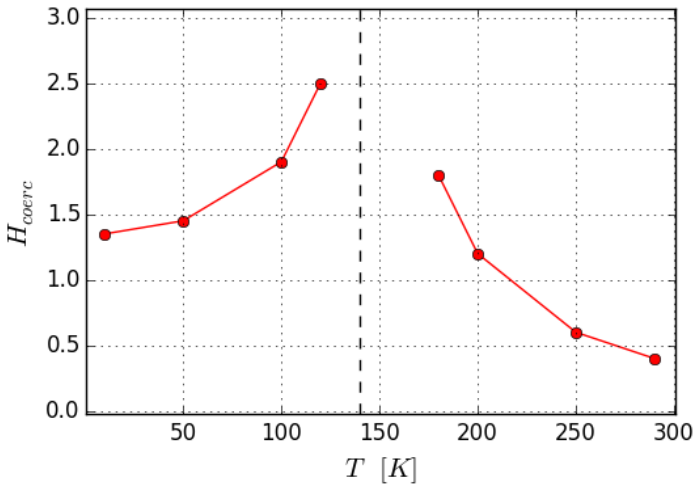


Figure 3.13: Coercive field as a function of the applied field for a set of different temperature above and below compensation.

From an intuitive point of view we can think that the field necessary to switch a magnetization is inversely proportional to the absolute value of the magnetization itself because the energy that a moment gains being parallel to an external field is proportional (see section 2.1.5) to the amplitude of the magnetic moment itself. Thus approaching compensation temperature the net magnetization of MRG decreases and thus it is less sensitive to the applied magnetic field. We expect that at compensation temperature the field that is necessary to switch the magnetization diverges. I did not have the chance to measure this sample very close to $T_{comp}$ in a magnet able to provide field higher than 4 T but in figure 3.14 it is shown an hysteresis loop carried out in a 14 T magnet exactly at compensation temperature, on a similar sample, by A. Jha in the ppms magnet in CRANN laboratory. Looking to figure 3.12 it can be noticed that the slope of the hysteresis loop is not flat neither in the high field part and we can assume that, at least far from compensation, the magnetization is completely saturated. Thus the slope that is still observable is due to Ordinary Hall effect which is induced by the fact that the external field is applied out of plane. Linearly fitting the high field part of the measurement it is possible to estimate the Ordinary Hall Resistance which is equal to the slope of the linear fit. It could be better noticed in figure 3.15.

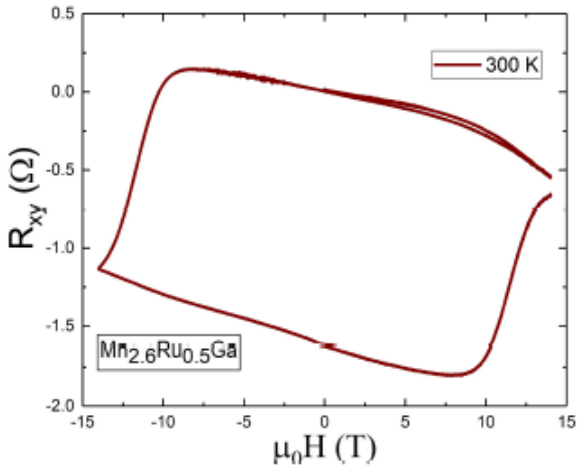


Figure 3.14: For this particular sample the compensation temperature was engineered to be at 300 K so the loop is done exactly at that critical temperature, indeed it could be seen that a magnetic field of 14 T is barely sufficient to switch the magnetization.

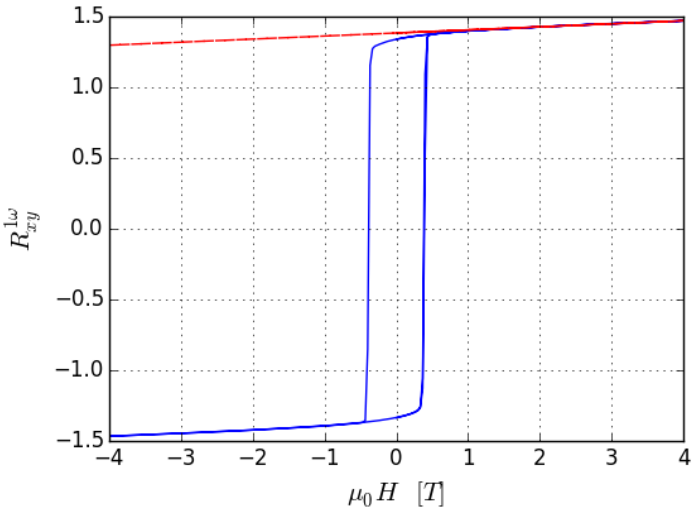


Figure 3.15: In blue the hysteresis loop at 290 K, the red dashed line is the linear fit of the high field part of the loop.

The slope of the high field fit is 22 $m\Omega/T$ and this represents the ordinary Hall Resistance. This effect will usually be neglected in this work because

the most important measurement are carried out using an in-plane field to tilt the magnetization with respect to the z-axis.

### 3.2.4 Determination of anisotropy constant

Exploiting X-ray and general magnetic characterization techniques we were able to determine the symmetry of the MRG crystal, thus, we can justify the expression of the magnetocrystalline anisotropy energy presented in section 2.1.5.
In order to simplify the total energy expression shown in equation 2.1.5.7 we have to do some further simplification regarding the exchange energy and the self-magnetic energy. In the model, that we used to explain and justify the experimental results obtained, is always assumed that the magnetization is saturated and applying an external magnetic field we are just modifying its equilibrium position. Within this assumption it is neglected the term in magnetic energy which is due to exchange interaction because we are assuming that all the atomic dipole moments are always parallel.
Further experiments shows that this is not strictly true considering especially the relative orientation of the Mn-4a and Mn-4c sublattices, however, since we are just tracking the projection of the Mn-4c sublattice along the z-axis,with magneto-transport measurement, this model works well enough.
Another important approximation that has to be done regards the self-magnetic energy, as it was explained in section 2.1.5, it is responsible in the determination of shape anisotropy. However in this sample the lattice strain forces the easy axis for the magnetization to lie out of plane, Neglecting all those terms the approximated expression for the total magnetic energy of the sample is:

$$E = k_1^{eff} sin^2(\theta) + k_1' sin^2(\theta) cos(4\phi) - \mu_0 \mathbf{H} \cdot \mathbf{M} \qquad (3.2.4.1)$$

Where the angles and axis orientation are shown in figure 3.9.
This expression clearly arises from a truncated Taylor expansion, thus, the second order term becomes more and more important when the magnetization is further tilted with respect to the z-axis. Since in this work the in-plane applied field is always chosen to do not induce a huge tilt in the magnetization we can further approximate the energy expression of equation 3.2.4.1 neglecting the second order term and replacing $k_1$ with $k_1^{eff}$ which takes into account also further terms of the expansion.
Defining also the magnetization in polar coordinates ($M_0$, $\theta$, $\phi$) we can ex-

press it as:

$$E = k_1^{eff} sin^2(\theta) + k_1' sin^2(\theta) cos(4\phi) \\ - \mu_0 M_0 (sin(\theta)cos(\phi)H_x + sin(\theta)sin(\phi)H_y + cos(\theta)H_z) \quad (3.2.4.2)$$

For each particular value of **H** calculating the minimums of the energy function is possible to obtain the equilibrium position for the magnetization of the sample as a function of the applied magnetic field.
In this position obviously holds:

$$\frac{\partial E(\theta_0, \phi, \mathbf{H})}{\partial \theta}) = 0 \; ; \; \frac{\partial E(\theta_0, \phi, \mathbf{H})}{\partial \phi} = 0 \quad (3.2.4.3)$$

Since we are going to characterize the magnetization of the sample measuring the Anomalous Hall Voltage we will obtain information just about the angle $\theta$ between the magnetization direction and the z-axis. Due to this fact the angle $\phi$ is not directly recorded and it is always assumed to be equal to $\text{arctg}(\frac{H_y}{H_x})$.
The strategy is to saturate the magnetization of the sample out of plane, then applying an in plane field and track how the magnetization changes as a function of the applied field.

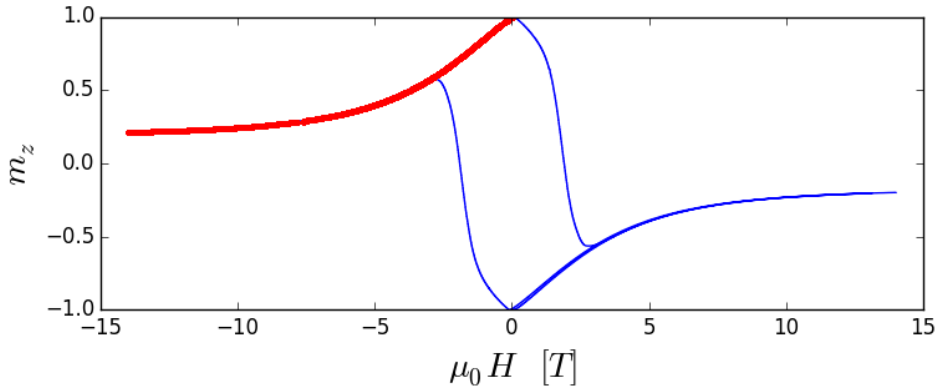


Figure 3.16: Field loop obtained in the ppms with the field in plane up to 14T. In red is highlighted the part of the field loop that is exploited to calculate the anisotropy constant.

Despite the field is assumed to be in the plane of the sample in figure 3.16 it can be noticed that there is a switching of the magnetization from positive

to negative direction. This is due to the not negligible tilt between the field direction and the actual plane of the sample, with a field that reaches 14 T also a small miss-alignment is enough to obtain an out of plane component of the field able to exceed the coercive field of the sample.
Exploiting a code developed by Ajay Jha it is possible to quantify the miss-alignment and then from that to reproduce what should be the ideal relation between $m_z$ and the in-plane applied field. Than from the resulting curve the effective anisotropy constant is extrapolated. For this sample, at room temperature it is obtained:

$$\frac{2k_1^{eff}}{\mu_0 M_s} \sim 2\ T \tag{3.2.4.4}$$

# Chapter 4

# Spin-Orbit Torque model and analysis

In paragraph 2.3.3 is shown how the symmetry of a particular lattice give rise to a preferential direction for the spin polarization of the conducting electron in a solid. The calculation was, explicitly, done for a tetragonal distortion of a cubic crystal. The same passages could be repeated for a perfectly cubic crystal ($4\bar{3}m$) and it would be obtained that in this case equation 2.3.3.1 reduces to:

$$\hat{\eta}(m) = \eta^{(1)} \begin{pmatrix} 0 & m_z & m_y \\ m_z & 0 & m_x \\ m_y & m_x & 0 \end{pmatrix} \tag{4.0.0.1}$$

For the development of the model that we used to characterize SOT the damping-like part of SOT is approximated to the one corresponding to a perfectly cubic lattice (equation 4.0.0.1). The resulting total tensor is:

$$\hat{\chi} = \hat{\chi}_{FL} + \hat{\chi}_{DL} = \chi_{FL} \begin{pmatrix} 1 & 0 & 0 \\ 0 & -1 & 0 \\ 0 & 0 & 0 \end{pmatrix} + \chi_{DL} \begin{pmatrix} 0 & m_z & m_y \\ m_z & 0 & m_x \\ m_y & m_x & 0 \end{pmatrix} \tag{4.0.0.2}$$

Which give rise to a polarization of the current flowing into the conductor according to the product of $\hat{\chi}$ times the current density vector $\mathbf{J}$.

$$\mathbf{S} = \hat{\chi}_{FL}\mathbf{J} + \hat{\chi}_{DL}\mathbf{J} \tag{4.0.0.3}$$

Due to a particular kind of itinerant exchange interaction [16] between free electrons and magnetic ions the magnetization of the material is perturbed from its equilibrium position. In order to model this effect usually an effective field is introduced, it is defined as the field necessary to tilt the magnetization from its equilibrium position to the one perturbed by the flow of a polarized

current.
This approach is particularly useful because the effective field ($\mathbf{H}_{eff}$) could be estimated comparing the tilt of the magnetization vector due to the current increase with the tilt of the magnetization due to an external applied field.

## 4.1 Tilt of the magnetization due to Spin Orbit Torque

In section 3.2.4 it is explained how to calculate the equilibrium value of $\theta$ as a function of the applied field, since we know that the Spin Orbit effective field perturbs this equilibrium we need to understand how the magnetization direction will evolve due to SOT.
In all the following discussion I will refer to the unperturbed value of $\theta$ and $\phi$ with $\theta_0$ and $\phi_0$ and to the perturbation of these with $\Delta\theta$ and $\Delta\phi$. The new equilibrium is defined by the following equation:

$$\frac{\partial E}{\partial \theta} = F(\theta_0 + \Delta\theta, \phi_0 + \Delta\phi, H_x^0 + H_x^{eff}, H_y^0 + H_y^{eff}, H_z^0 + H_z^{eff}) = 0 \quad (4.1.0.1)$$

Where F is defined as the partial derivative of the total energy with respect to $\theta$, $H^0$ is the external applied field and $H^{eff}$ is the effective field due to SO interaction.
In order to solve this equation we have to neglect $\Delta\phi$, we are allowed to do this because it influences the Anomalous Hall Voltage just indirectly due to the variation of $\theta$ connected to the change of $\phi$ trough the four fold anisotropy. Using some typical value [36] for $\hat{\chi}_{fl}$ and $\hat{\chi}_{dl}$ we obtain an effective field due to SOT which is small if compared with the applied one, due to this fact we can calculate the new equilibrium value of $\theta$ expanding F around the unperturbed equilibrium point

$$\begin{aligned} F(\theta, \phi, H_x, H_y, H_z) &= 0 \\ &= \cancel{F(\theta_0, \phi_0, H_x^0, H_y^0, H_z^0)} \\ &\quad + \left( \frac{\partial F}{\partial \theta}\Delta\theta + \frac{\partial F}{\partial H_x}H_x^{eff} + \frac{\partial F}{\partial H_y}H_y^{eff} + \frac{\partial F}{\partial H_z}H_z^{eff} \right) \\ &\quad + \frac{1}{2}\left( \frac{\partial^2 F}{\partial \theta^2}\Delta\theta^2 + 2\frac{\partial^2 F}{\partial \theta \partial H_x}\Delta\theta H_x^{eff} + 2\frac{\partial^2 F}{\partial \theta \partial H_y}\Delta\theta H_y^{eff} \right. \\ &\quad \left. + 2\frac{\partial^2 F}{\partial \theta \partial H_z}\Delta\theta H_z^{eff} \right) \end{aligned} \quad (4.1.0.2)$$

In the expansion do not appear all the terms in which there is a second derivative of F with respect to the H field because F dependence is linear in the field so they are all null.
Equation 4.1.0.2 is a second order equation in $\Delta\theta$ and after some algebraic calculation it could be obtain the expression of $\Delta\theta$ induced by the current.

$$\Delta\theta = -\frac{1}{\frac{\partial F}{\partial \theta}}(\boldsymbol{v}_1 \cdot \boldsymbol{H}^{eff}) - \frac{1}{2(\frac{\partial F}{\partial \theta})^2}(\boldsymbol{v}_1 \cdot \boldsymbol{H}^{eff})(\boldsymbol{v}_2 \cdot \boldsymbol{H}^{eff}) \tag{4.1.0.3}$$

Where $\boldsymbol{v}_1$ and $\boldsymbol{v}_2$ are defined as follow

$$\boldsymbol{v}_1 = \begin{pmatrix} \frac{\partial F}{\partial H_x} \\ \frac{\partial F}{\partial H_y} \\ \frac{\partial F}{\partial H_z} \end{pmatrix} \quad ; \quad \boldsymbol{v}_2 \begin{pmatrix} 2\frac{\partial^2 F}{\partial \theta \partial H_x} - \frac{\partial^2 F}{\partial \theta^2}\frac{\partial F}{\partial H_x}\frac{1}{\frac{\partial F}{\partial \theta}} \\ 2\frac{\partial^2 F}{\partial \theta \partial H_y} - \frac{\partial^2 F}{\partial \theta^2}\frac{\partial F}{\partial H_y}\frac{1}{\frac{\partial F}{\partial \theta}} \\ 2\frac{\partial^2 F}{\partial \theta \partial H_z} - \frac{\partial^2 F}{\partial \theta^2}\frac{\partial F}{\partial H_z}\frac{1}{\frac{\partial F}{\partial \theta}} \end{pmatrix} \tag{4.1.0.4}$$

And considering the fact that the effective field linearly depends on the current density we can rewrite it as:

$$\Delta\theta = d\theta_1 j + d\theta_2 j^2 \tag{4.1.0.5}$$

## 4.2 Characterization of SOT by Anomalous Hall Effect

In order to measure the effect that the current induced effective field has on the magnetization of a particular material we measure the transversal voltage across an Hall bar.

$$V_{xy}^{AH} = R_{xy} I cos(\theta_0 + \Delta\theta) = \frac{\rho_{xy}}{t} I cos(\theta_0 + \Delta\theta) = \frac{\sigma_{xy}}{\sigma_{xx}^2 + \sigma_{xy}^2}\frac{I}{t} cos(\theta_0 + \Delta\theta) \tag{4.2.0.1}$$

Where $\Delta\theta = d\theta_1 j + d\theta_2 j^2$.
And considering that $\sigma_{xy} << \sigma_{xx}$ we can rewrite:

$$V_{xy}^{AH} = \frac{\sigma_{xy}}{\sigma_{xx}^2}\frac{I}{t} cos(\theta_0 + \Delta\theta) = \frac{\sigma_{xy}}{\sigma_{xx}^2}\frac{I}{t}\left[cos(\theta_0)cos(\Delta\theta) - sin(\theta_0)sin(\Delta\theta)\right] \tag{4.2.0.2}$$

Now assuming that the $\Delta\theta$ is a small quantity we can expand the sinusoidal functions around the origin obtaining:

$$V_{xy}^{AH} = \frac{\sigma_{xy}^0}{(\sigma_{xx}^0)^2}\frac{I}{t}\left[cos(\theta_0) - cos(\theta_0)\frac{d\theta_1^2 I^2}{2w^2 t^2} - sin(\theta_0)\left(\frac{d\theta_1 I}{wt} + \frac{d\theta_2 I^2}{w^2 t^2}\right)\right] \tag{4.2.0.3}$$

Considering that $I = I_{ac}sin(\omega t)$ all the terms that are multiplied by $I^3$ will appear on the third harmonic since

$$I = (Isin(\omega t))^3 = \frac{I_{ac}^3}{4}(sin(3\omega t) - 3sin(\omega t)) \tag{4.2.0.4}$$

Observing equation 4.2.0.4 it can be seen that the third power of a sinusoidal current, in the harmonics expansion give rise to two different harmonic signal, one at the same frequency of the current ($\omega$) and one on the third harmonic ($3\omega$). Keeping just the terms that appear on the third harmonic after simple calculation we can find the expression of the expected signal.

$$V_{xy}^{3\omega} = -I_{ac}^3 \left[ \frac{cos(\theta_0)\sigma_{xy}^0 d\theta_1^2}{(\sigma_{xx}^0)^2 8w^2t^3} + \frac{sin(\theta_0)\sigma_{xy}^0 d\theta_2}{(\sigma_{xx}^0)^2 4w^2t^3} \right] \tag{4.2.0.5}$$

In order to perform a proper analysis it has to be considered the fact that the conductivity is not constant as a function of the current. This non-ideal behavior is related to the fact that electrons flowing into the material collide with the ions of the lattice and this produces a global increase of the temperature.

$$\Delta T = \chi I^2 \rightarrow \sigma = \sigma_0 + \frac{\partial \sigma}{\partial T}\Delta T \tag{4.2.0.6}$$

From this consideration it is clear that when the total conductivity is multiplied times the current in order to get the voltage, this non ideality produces a term in which appears the current to the third power and, as shown in equation 4.2.0.4, this will be demodulated together with the SOT signal on the third harmonics.
In order to correctly analyze the results it has to be estimated the $\Delta T$ induced by a certain current density and also the behavior of $\sigma_{xx}$ and $\sigma_{xy}$ as a function of temperature. In the supplementary material of [36] it is well explained how to properly consider the heating effect in the analysis of the results. In order to estimate the field-like and damping-like coefficient a code was implemented with the model previously explained and the results for two particularly significant situation are shown in figure 4.1 where the direction of the current is parallel to the x axis.

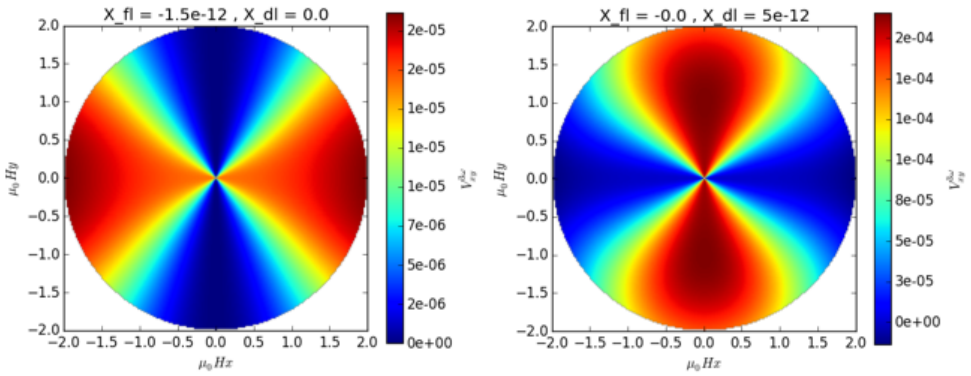


Figure 4.1: Both the picture are not meaningful from a quantitative point of view because is not considered the heating effect. The $V_{xy}^{3\omega}$ is calculated just from the expression 4.2.0.5 exploiting right values for all the parameters that appear in the expression. The current direction is parallel to the x-axis

From this two figures is clear that if the field-like (FL) SOT is dominant the $\Delta\theta$ is parallel to the current direction while if the damping-like (DL) torque is dominant the effect is mainly perpendicular to the current direction.
Exploiting the result of an hall measurement at an high current is thus possible to understand if which between FL and DL torque is dominant.

## 4.3 Harmonic analysis

This section is devoted to properly understand what are the different signal expected on the harmonic of interest. In order to keep the notation easier I will express the voltage in terms of current times the resistance instead of using the conductivity.

$$V_{xy}^{AH} = R_{xy} I(t) cos(\theta_0 + \Delta\theta) \tag{4.3.0.1}$$

From all the calculation of the previous section it is known that the total anomalous hall signal is composed by terms proportional to $I(t)$, $I^2(t)$ and $I^3(t)$ where $I(t) = I_0 sin(\omega t)$.

$$\begin{aligned} V_{xy}^{AH} = R_{xy} \Bigg[ & I(t) cos(\theta_0) - I^2(t) sin(\theta_0) \frac{d\theta_1}{wt} \\ & - I^3(t) \left( cos(\theta_0) \frac{d\theta_1^2}{2w^2t^2} + sin(\theta_0) \frac{d\theta_2}{w^2t^2} \right) \Bigg] \end{aligned} \tag{4.3.0.2}$$

And substituting now to all the power of I(t) the relative harmonic expansion we can rewrite the signal expected on each different $\omega$

$$V_{xy}^{1\omega} = I_0 R_{xy} cos(\theta_0) - 3V_{xy}^{3\omega} \tag{4.3.0.3}$$

$$V_{xy}^{2\omega} = \frac{1}{2} I_0^2 sin(\theta_0) d\theta_1 \tag{4.3.0.4}$$

$$V_{xy}^{3\omega} = \frac{1}{4} I_0^3 R_{xy} \left[ cos(\theta_0) d\theta_1^2 + sin(\theta_0) d\theta_2 \right] \tag{4.3.0.5}$$

Observing equation 4.3.0.3 it is clear that in the approximation that the effective field is linear with the current density and $d\theta << \theta_0$ on the first harmonic SOT effects appears just because of the presence in $sin^3(\omega t)$ of a term which oscillates at $\omega$ (equation 4.2.0.4). Because of this reason after summing $3V_{xy}^{3\omega}$ to $V_{xy}^{1\omega}$ the first harmonic signal is expected to be free from all the effects that arise from the linear part of spin orbit torque.

$$R_{xy} cos(\theta_0) = \frac{V_{xy}^{1\omega} + 3V_{xy}^{3\omega}}{I_0} \tag{4.3.0.6}$$

In the next section will be properly studied with a different approach the linear and the non-linear part of SOT and it will be presented a qualitative explanation of the observed existence of a strongly non-linear Spin Orbit Torque.

# Chapter 5

# Experimental result

The experimental work related to this thesis was mainly composed by two different parts. In the first period the measurement were performed exploiting a cryomagnet able to provide a stable magnetic field from 0 to 4T, along a fixed direction, integrated with a cryostat working from 10K to 310K. The superconductor magnet is continuously cooled exploiting a closed loop of helium. In this part of the work we carefully characterized the temperature dependence of longitudinal and transversal conductivity. This was necessary in order to distinguish between the effect of heating and the effect of Spin Orbit Torque on the third harmonic signal resulting from a typical hall measurement.
The second part, which is the core of the work, was related to the investigation of the non linear part of Spin Orbit effective field as a function of current. These experiments were performed at room temperature in a multimag able to provide a rotating field up to a maximum of 2T.

## 5.1 Linear part of SOT field

This part of the work was the first one in which I participated when I started my research experience in Trinity College.
The goal was to characterize the linear contribution of the effective field to the Spin Orbit performing analysis on the third harmonic.
The sample that have been used is slightly different with respect to the one on which are based all the measurement showed in section 3. The magnetic and crystallographic properties are however very similar and they are properly summarized at [36].

### 5.1.1 Quantification of heating effect and SOT linear parameters

Resuming all the considerations that have been done in section 4.2 about the existence of a term, due to heating effect, superimposed to SOT on the third harmonic the total expression of $V_{xy}^{3\omega}$ is:

$$(V_{xy}^{TOT})^{3\omega} = -I_{ac}^{3}\left[\frac{cos(\theta_0)\sigma_{xy}^{0}d\theta_1^2}{(\sigma_{xx}^{0})^2 8w^2t^3} + \frac{sin(\theta_0)\sigma_{xy}^{0}d\theta_2}{(\sigma_{xx}^{0})^2 4w^2t^3} - \frac{cos(\theta_0)\beta^0\chi}{(\sigma_{xx}^{0})^2 4t} + \frac{cos(\theta_0)\alpha^0\chi\sigma_{xy}^{0}}{(\sigma_{xx}^{0})^3 2t}\right] \tag{5.1.1.1}$$

Where $\alpha^0$ and $\beta^0$ are defined as follow:

$$\alpha^0 = \frac{\partial\sigma_{xx}^{0}}{\partial T} \;\; and \;\; \beta^0 = \frac{\partial\sigma_{xy}^{0}}{\partial T} \tag{5.1.1.2}$$

Looking to equation 5.1.1.1 it can be understood that in order to get some quantitative information about $\mathrm{d}\theta_1$ and $\mathrm{d}\theta_2$ it is necessary to estimate $\alpha_0$, $\beta_0$ and $\chi$.
I participated in the acquisition of these data that later have been used to separate the SOT signal from the heating effect on the third harmonic of an Hall measurement through the model presented above.
$\alpha^0$ and $\beta^0$ are directly obtained differentiating traversal and longitudinal conductivity as a function of temperature and the resulting functions are shown in figure 5.1 (c) and (d).
In order to estimate $\chi$ the plot shown in figure 5.1 (a) and (b) are compared with the change in conductivities resulting from the injection of an high current density. This allowed us to obtain an effective, current induced, increase of temperature looking to the change of conductivity and from $\Delta T$ through equation 4.2.0.6 it is possible to obtain $\chi$ which approximately is $\chi \sim 4 \cdot 10^5$. This results from a change of temperature of $\Delta T \sim 15K$ when the current passes from 0.1 mA to 10 mA.

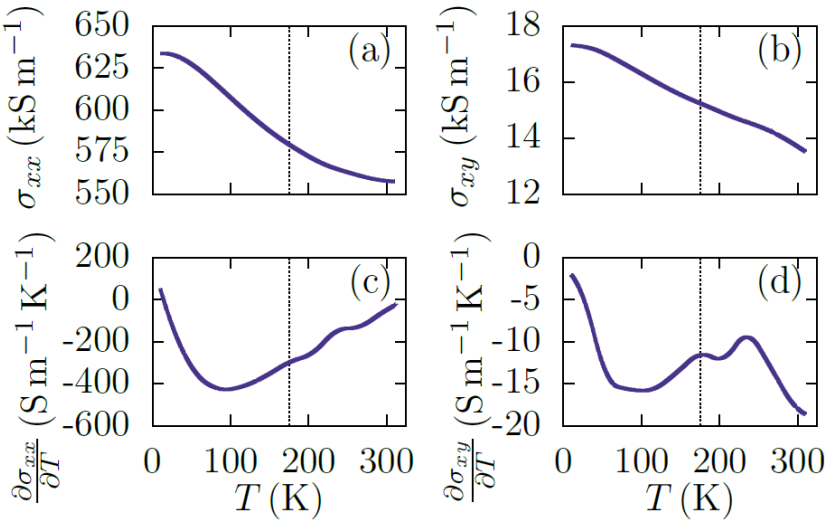


Figure 5.1: The measurement are carried out with a very low current density in order to neglect the heating effect due to such a low current. The applied magnetic field during the experiment was null and the sample was magnetized just before the start of the measurement.

As expected both the conductivities decrease as a function of temperature and in particular in $\sigma_{xx}$ it is possible to observe that the conductivity starts to saturate at high temperature.
Observing the behavior of $\sigma_{xy}$ it is interesting to notice that the decrease is almost linear and this is in accord with the fact that the hall conductivity basically tracks the Mn-4c lattice magnetization which is linearly decreasing as a function of temperature.
In order to obtain some quantitative values for field-like and damping-like constant the strategy was to compare the simulation done with the developed model and the experimental data previously obtained.
The scheme of the experiment was to use the multimag in order to produce a field in the plane of the sample and tilt the magnetization from its out of plane equilibrium position. The field was programmed to span from 0 to 2 T on step of 0.1 T and for each step a $\phi$ scan was performed.
The first data were collected at very low current density ($1 \cdot 10^8$ $A/m^2$) in order to measure the equilibrium position of the magnetization without any contribution from the Spin Orbit field. Practically from the low current scan it was calculated $\theta_0$ which appears in equation 5.1.1.1. Then the current density was gradually increased and on the high current scan it was subtracted the heating effect. Then comparing the simulation and the experimental results an estimation of field-like and damping-like parameter was obtained.

In figure 5.2 a) is shown the experimental results with a current density of $2.5 \cdot 10^{10} \mathrm{A/m^2}$ parallel to the y-axis which has to be compared with the simulation on the right (where $\theta_0$ is extracted from the low current scan) in order to estimate the parameters of interest.

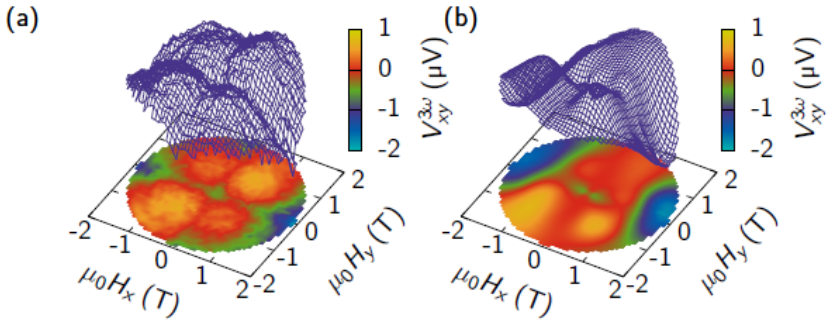


Figure 5.2: Comparison between the experimental signal recorded on the third harmonic and the expected signal calculated using equation 5.1.1.1 with some suitable values of $x_{FL}$ and $x_{DL}$.

The best agreement between the measurement and the model is shown in 5.2 and is achieved with the following parameters for the Spin Orbit effective field.

$$x_{FL} = 15 \cdot 10^{-13}\, TA^{-1}m^2 \qquad x_{DL} = 50 \cdot 10^{-13}\, TA^{-1}m^2 \tag{5.1.1.3}$$

To summarize the coefficients that relate the current density with the effective field through equation 4.0.0.2 and 4.0.0.3 have been estimated and the heating due to the high current density was properly taken into account.
During this part of the work I was trained in the use of the experimental setup trough the measurement that we performed about the quantification of the heating effect. The measurement devoted to the actual estimation of SOT were already completed,and we performed some measurement needed to correctly take into account the heating effect due to current.

## 5.2 Non linear character of SOT at room temperature

As it is explained in section 4.3 the recorded signal on the third harmonic can be manipulated in order to get rid of all the linear SOT part coming from the third harmonic. In order to investigate the non-linear behavior of

the effective field we investigated this signal employing a very high current density ($J \sim 1 \cdot 10^{10}\mathrm{A/m^2}$).
For this experiment we used the sample which characterization is shown in section 3.1, we patterned two different device varying the current direction.In the first study it was parallel to [100] crystallographic axis of MRG while in the second device the current direction was parallel to [110] crystallographic axis.

### 5.2.1 [100] pattern

For this particular pattern the current density vector is defined as:

$$\mathbf{J} = J_0 \begin{pmatrix} 1 \\ 0 \\ 0 \end{pmatrix} \tag{5.2.1.1}$$

Exploiting the equivalence between a polarization of the electronic current and an effective magnetic field, according to equations 4.0.0.2, 4.0.0.3 and with the current density defined as in equation 5.2.1.1, it is obtained that the effective field is:

$$\mathbf{h}_{eff} = \begin{pmatrix} x_{FL} J_0 \\ x_{DL} m_z J_0 \\ x_{DL} m_y J_0 \end{pmatrix} \rightarrow \begin{pmatrix} x_{FL} J_0 \\ x_{DL} m_{oop} J_0 \\ x_{DL} m_{ip} J_0 \end{pmatrix} \tag{5.2.1.2}$$

It is important to precise that because of the tetragonal symmetry of the MRG crystal the x-axis is perfectly equivalent to the y-axis. It is better to refer to a generic in-plane magnetization rather than to $m_x$ or $m_y$.
The goal of the following measurements was to characterize the intensity of the non-linear effective field as a function of the current density and the ratio between in plane and out of plane magnetization ($\mathrm{m}_{ip}/\mathrm{m}_{oop}$).
The strategy of the whole experiment was to decide some significant values for the applied in plane field and then for each step rotate the field in the plane of the sample. For each step of the field the current density was increased from $5 \cdot 10^8\mathrm{A/m^2}$ to $5 \cdot 10^{10}\mathrm{A/m^2}$.

Figure 5.3: 2 T multimag system.

In figure 5.3 it is shown a picture of the 2 T multimag. The film was mounted parallel to the floor and the magnetic field is rotated in the plane of the sample. This magnet is not integrated with a cryostat so all the measurement were performed at room temperature and atmospheric pressure, which enhances the heat dissipation and allowed us to test the material up to very high current density without burning the sample.

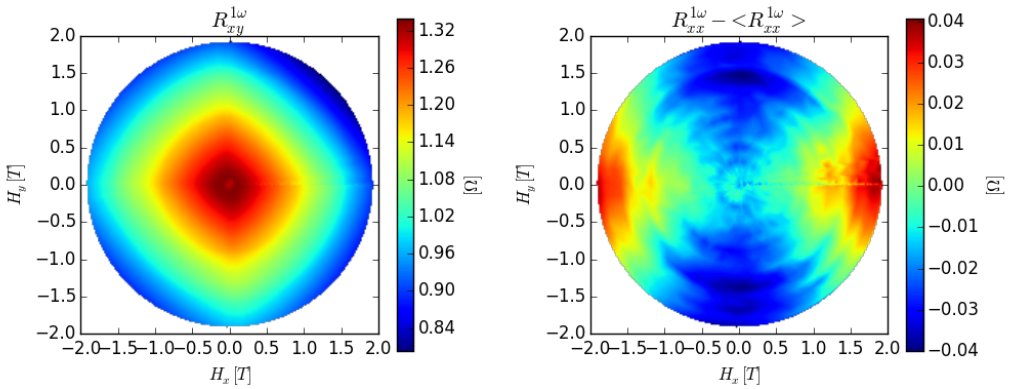


Figure 5.4: Low current field scan. The current was set to 0.3 mA with a frequency of 517 Hz while each field point was chosen with amplitude step of 0.1 T (from 0 to 2 T) and angular step of $6^o$. On the left a 2D representation of the anomalous hall voltage normalized on the current. On the right a representation of the variation of the longitudinal resistance with respect to the average value of the signal.

In figure 5.4 can be recognized (on the left) the effect of the four fold anisotropy previously discussed (section 2.1.5). The crystal had already been

studied with crystallographic measurement to confirm that the structure was the expected one, with this data we can confirm that also the magnetic state behaves as expected. From a magnetic energy point of view the minima are placed at $45^o$, $135^o$, $225^o$ and $315^o$. Looking to the right image of figure 5.4 it is clearly shown the effect of the Anisotropic Magnetoresistance (see section 2.2.2). The difference in resistance between parallel or perpendicular relative orientation of current and magnetization is very small ($\sim 0.08\Omega$) but is enough to confirm us that, mounting the sample, the hall bar was correctly positioned with the current direction parallel to the x-direction of the magnetic field. In the picture it is subtracted the average value of the longitudinal resistance (266 $\Omega$) just to make clearer the AMR effect. This result is also important because it confirms that it is perfectly allowed to neglect this effect in the SOT analysis because $\frac{0.08\Omega}{266\Omega} << 1$.
In figure 5.5, for some significant current amplitude and at six different values of the in plane magnetic field, it is shown the signal recorded on the first harmonic plus three times the signal recorded on the third harmonic. As explained in section 4.3 this operation is needed to remove all the contribution arising from the linear part of the SOT present on the first harmonic of an Hall measurement.

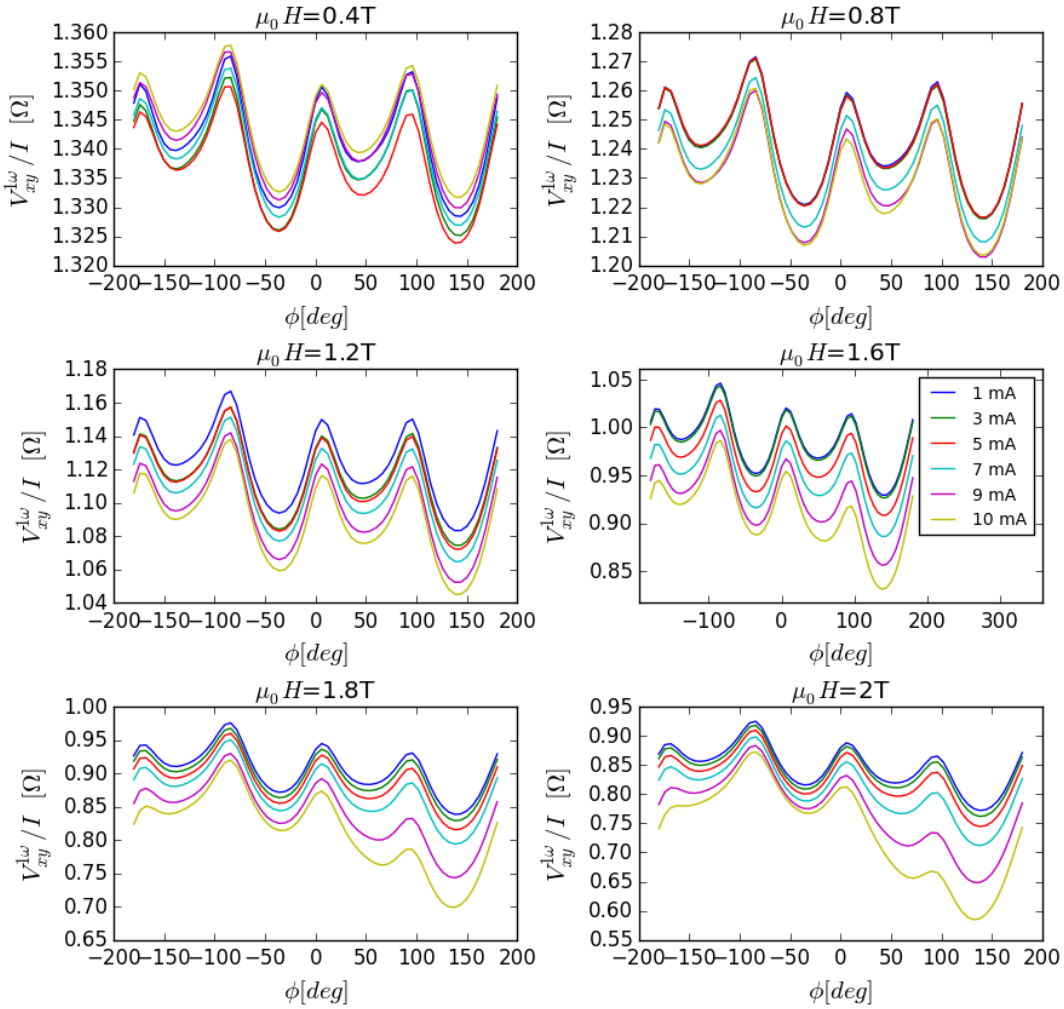


Figure 5.5: In each subplot is shown $(V_{xy}^{1\omega} + 3V_{xy}^{3\omega})/I_0$ for I=1mA, I=3mA, I=5mA, I=7mA, I=8mA, I=10mA.

It can be noticed that in all the pictures there is a small constant shift due to the heating effect, it will be subtracted in the final analysis fitting with a second order polynomial the average values of the scan at low current (before SOT shows-up) . For the plot at 0.4T, 0.8T, and 1.2T the plot of the different current have all the same shape while in the other three plots the high current data have a shape that is distorted with respect to the low current measurement. In order to ensure that this difference was not due to a degradation of the magnetic state for each of the six field, after the highest current measurement, a low current scan was performed in order to check

that it overlaps with the previous ones.
This particular behavior was not predicted by the model explained in section 4.1, it means that one or more hypothesis are not actually true for high value of the current density.
We will refer to this effect as "Non linear part of SOT" since the linear contribution is removed and everything else showing some difference in the magnetization equilibrium position for high current density is arising from some non linearity in the definition of the effective field.
Namely it means that with respect to the definition of $\chi$ reported in equation 4.0.0.2 we have to consider that the magnetization ($m_x$, $m_y$, $m_z$) can not be considered constant as a function of current and the effective field definition changes.

$$\mathbf{h}_{eff} = \chi_{FL} \begin{pmatrix} 1 & 0 & 0 \\ 0 & -1 & 0 \\ 0 & 0 & 0 \end{pmatrix} \cdot \mathbf{J} + \chi_{DL} \begin{pmatrix} 0 & m_z(\mathbf{J}) & m_y(\mathbf{J}) \\ m_z(\mathbf{J}) & 0 & m_x(\mathbf{J}) \\ m_y(\mathbf{J}) & m_x(\mathbf{J}) & 0 \end{pmatrix} \cdot \mathbf{J} \tag{5.2.1.3}$$

In this way it is possible to take into account the fact that an high effective field modifies the magnetization equilibrium such that the damping-like part of the effective field changes because it directly depends on the magnetization.
In order to estimate the non-linear effective field the strategy was to firstly obtain the behavior of the magnetization as a function of the applied in-plane field and then to invert it. Doing this it is possible to explicit what is the necessary applied in-plane field to obtain a certain value of the magnetization along z-axis. This makes possible to estimate the effective field comparing what is the expected field value to obtain a certain $m_z$ with the actual applied field.
We initially focus on the experiment with an in-plane field of 2T because it is the situation in which this effect is more evident trying to estimate the non-linear effective field as a function of the current density.
From now on all the transversal resistance are normalized to the highest value (magnetization parallel to z), it means that this normalized Hall signal is perfectly equivalent to the normalized magnetization $m_z = M_z/M_s$.

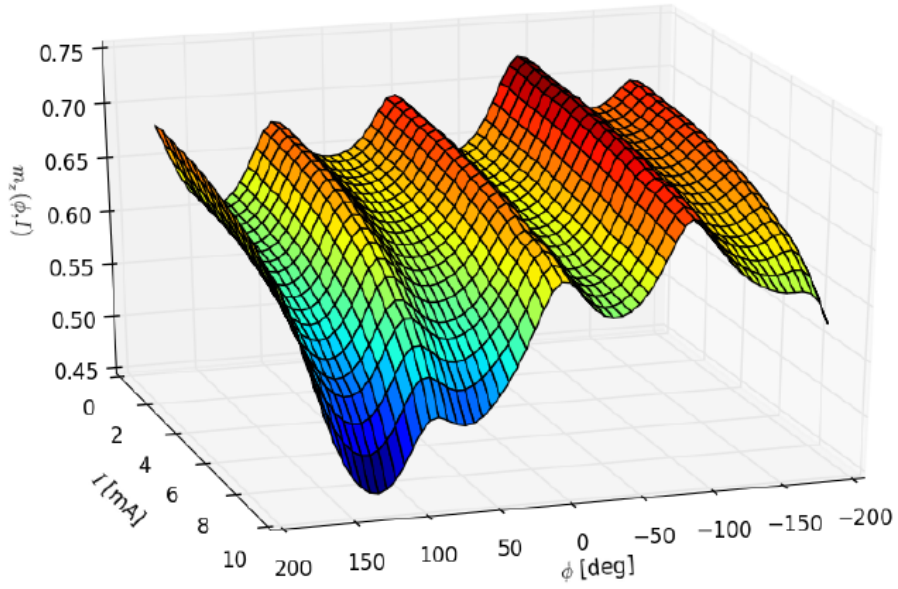


Figure 5.6: Plot of $m_z$ for all the current used to characterize SOT in the sample. It can be noticed that when the current is greater than 5 mA there is an evident shift of the actual $m_z$ with respect to the one recorded at low current.

In order to visualize the angular dependence of non-linear SOT we firstly remove the low current measurement from the high current one (figure 5.7). On the third dimension of the plot in figure 5.7 it is basically shown the $\Delta m_z$. It represents the difference in magnetization along z with respect to the low current measurement.
We observe that for the highest value of the current density ($5{\cdot}10^{10} Am^{-2}$) $\Delta m_z$ is about 0.15 which compared to a unitary magnetization is a huge value.

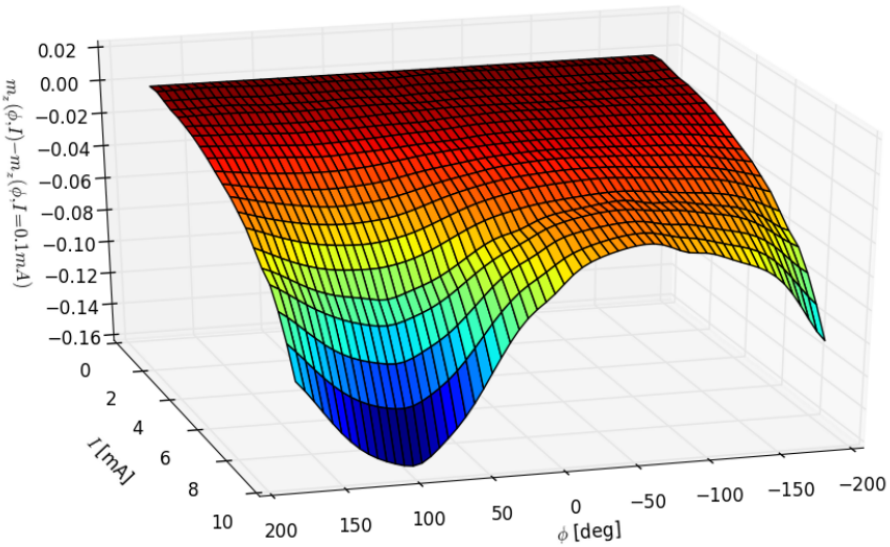


Figure 5.7: The figure shows $m_z(\phi, I) - m_z(\phi, I = 0.1mA)$. From all the measurement the $m_z$ recorded for the lowest current is subtracted to al the others recorded $m_z$ in order to make more clear the effect of Spin Orbit field. The maximum difference is achieved for an angle about $100^o$.

In order to relate this $\Delta m_z$ with an effective field we exploited a curve showing the applied in plane field as a function of the magnetization.

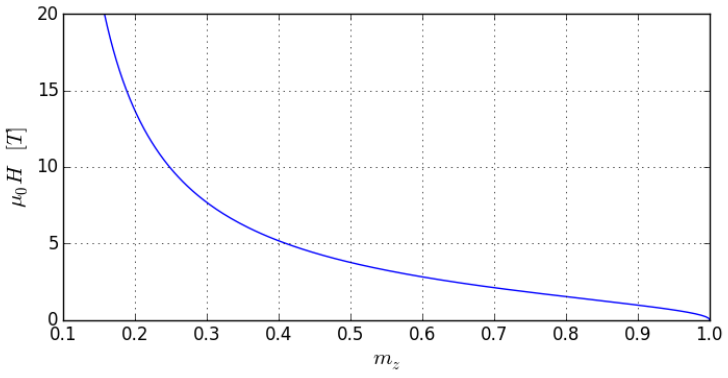


Figure 5.8: Applied in-plane field plotted as a function of $m_z$.

Exploiting the plot showed in figure 5.8 it is possible to obtain a quantitative estimation of the non-linear spin orbit field. For example for field amplitude fixed to 2 T the expected value for $m_z$ is about 0.7 which is verified

for scan up to 5 mA ($2.5{\cdot}10^{10} A/m^2$) than the $\Delta m_z$ due to non-linear SOT start to be observable.
A zoomed version of figure 5.8 is shown in figure 5.9 to make clearer the calculation of the effective field.

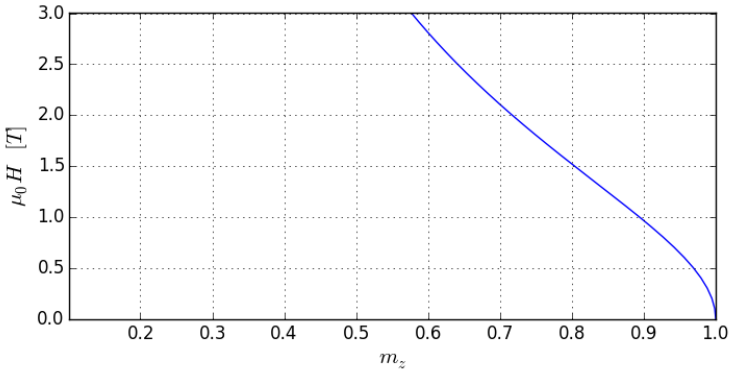


Figure 5.9: Zoom of figure 5.8 from 0 to 3 T.

Starting from $m_z = 0.71$ which is the $m_z$ obtained with low current measurement and 2 T of applied field we consider the results previously calculated of $\Delta m_z = -0.15$ it means that the field which should be necessary to obtain an $m_z = 0.57$ is 3 T. From this simple argument it is possible to quantify the maximum effective field for a current density of $5{\cdot}10^{10} a/m^2$ and an applied field of 2T which is about $h_{eff} \sim 1T$.
Repeating this calculation for all the current density and all the possible $\phi$ angles it is obtained the behavior of the non-linear effective field as a function of current and direction.

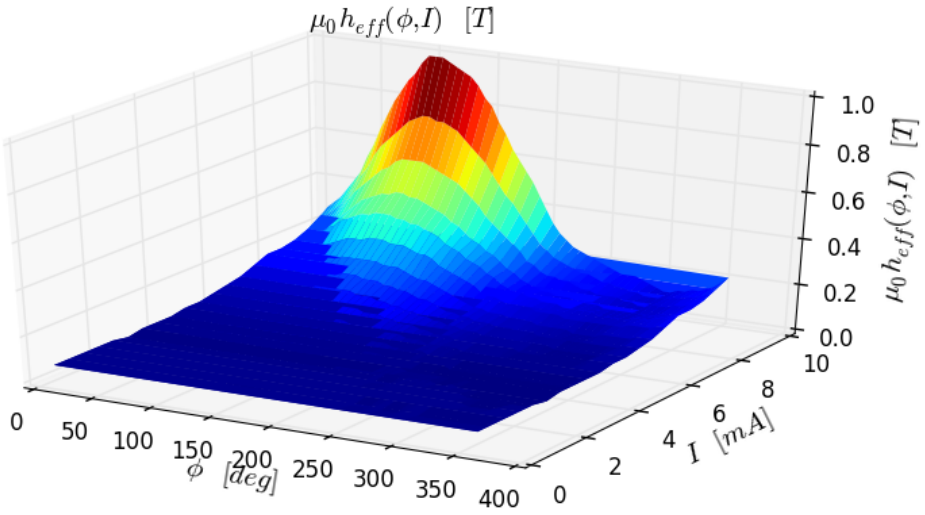


Figure 5.10: Graphical representation of the effective field as a function of the current and the magnetization direction ($\phi$). It is plotted as a function of current intensity instead of current density to make it clearer, the equivalence is obtained simply dividing by the section, which is $20nm \times 10\mu m$.

As it was possible to notice from also from the previous figures the maximum effect of the non-linear Spin Orbit effective field is achieved when the magnetization is almost perpendicular to the current. It is also evident that the effect becomes not negligible when the current exceeds 6mA (3 A/m$^2$) and then the increment is definitely non-linear.
At this point the same calculation was repeated for all the others amplitude of the applied in-plane field and, as could have been already predicted from figure 5.5 the effective field has always the same symmetry, with the peak obtained when the magnetization vector is perpendicular to the current direction and its maximum value quickly decreasing until SOT effect disappears at 0.8 T of applied in plane field.
As a final result in figure x it is represented the behavior of the effective field as a function of the amplitude of the applied in plane field.

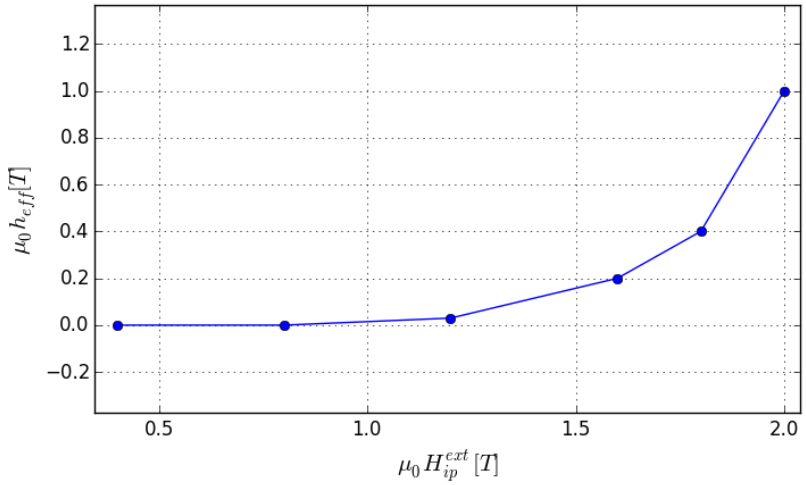


Figure 5.11: .

At this point some consideration has to be done regarding the behavior of the effective field shown in 5.11. It seems from that picture that the effective field is increasing as the in-plane magnetization increases. This suggests that, looking to equation 5.2.2.1, the component of the effective field that is more relevant is the one directed along z-axis, because it is the unique one that is proportional to the in-plane magnetization.
We realize that in order to properly characterize the effective field we would have to map the behavior of $m_z$ not just as a function of the in plane applied field but as a function of a field which rotates around all the possible $\theta$ directions and varies also its intensity.
In this way we would be able to have some information also about the out of plane effective field. Unfortunately because of the geometry of such an experiment it results quite complicated and probably it should be used the ppms system which is able to provides an, high enough, field and to rotate it among all the direction of interest.

### 5.2.2 [110] pattern

After we finished the characterization of the non-linear part of SOT on such device a new one was patterned with a different current direction in order to complete the study.
The experiment performed is exactly the same explained and analyzed in the previous section but the Hall bar used has a different current direction with respect to the crystallographic axis. The current now flows parallel to the [110] direction of the MRG crystal.
The expression of the effective field becomes:

$$\mathbf{h}_{eff} = \frac{x_{FL}J_0}{\sqrt{2}} \begin{pmatrix} 1 \\ 1 \\ 0 \end{pmatrix} + \frac{x_{DL}J_0}{\sqrt{2}} \begin{pmatrix} m_Z \\ m_z \\ m_x + m_y \end{pmatrix} \tag{5.2.2.1}$$

Since the method to analyze the data is exactly the same I will present just the most important results.
The angle $\phi$ is in this case defined with the 0 perpendicular to the current direction.

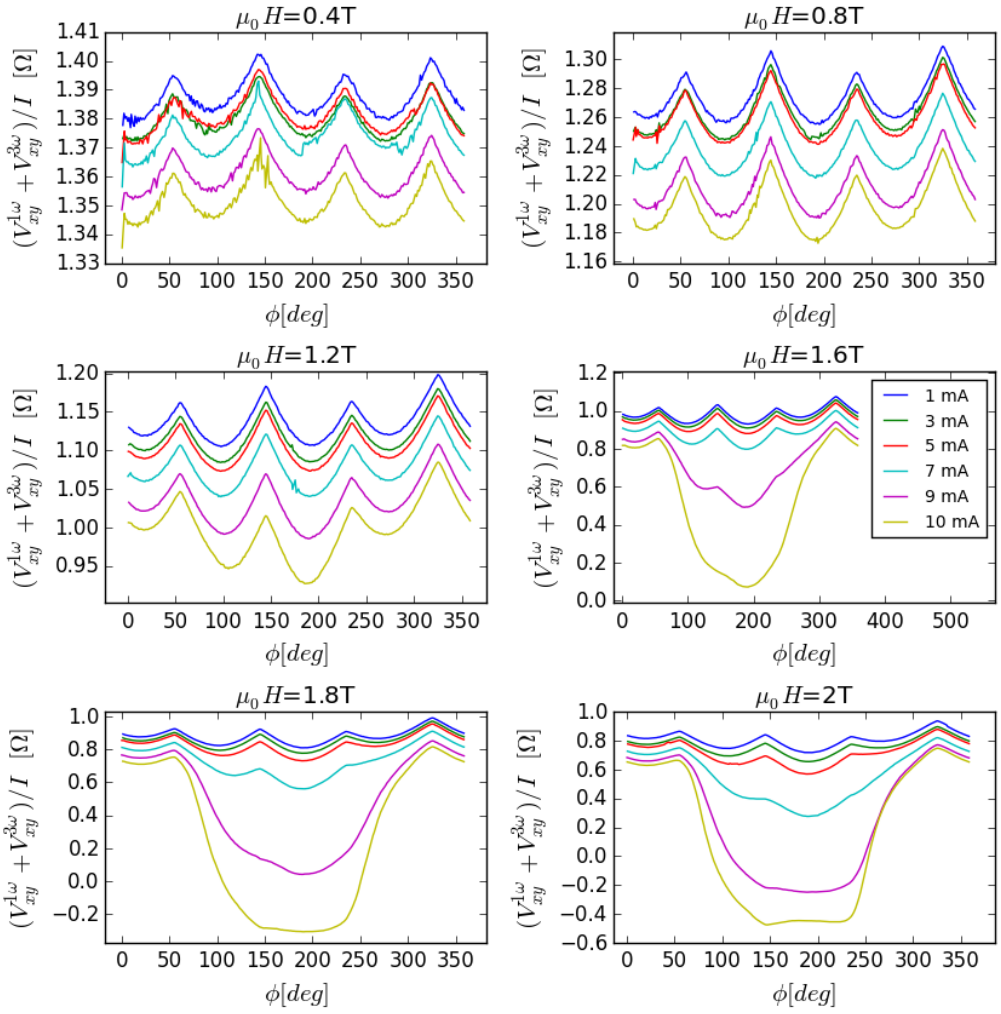


Figure 5.12: In each subplot is shown $(V_{xy}^{1\omega} + 3V_{xy}^{3\omega})/I_0$ for I=1mA, I=3mA, I=5mA, I=7mA, I=9mA, I=10mA.

As for the experiment previously analyzed the scans performed with a magnetic in plane field lower than 1.2T do not show any noticeable effect of spin orbit torque, neither at the maximum current while for in plane field higher than 1.2T already with 5 mA the effect of current induced spin polarization is evident.
The signal showed in figure 5.12 was then normalized and thus could be considered as the normalized magnetization along the z-axis. As for the previous analysis the heat was fitted with a second order polynomial and then removed from the whole plot.

Looking to $m_z$ it can be noticed that at high current density, for in plane field of 1.8 T and 2 T, the effect of SOT is such strong that it induces partial switch of some domains.
Focusing this result and the consideration done at the end of the previous section regarding the real origin of the effective field it results that it is impossible to model this situation just with the existence of an in plane effective field. Such a field supposed in the plane of the sample would not be able to induce any switch so in order to proper analyze those situation it would be needed a precise map of $m_z$ as a function of the amplitude and $\theta$ of an applied field. With the results currently available, it is better to focus on the scans done at 1.6 T of applied in plane field in which $m_z$ remains always positive but is still strongly influenced from non-linear SOT.

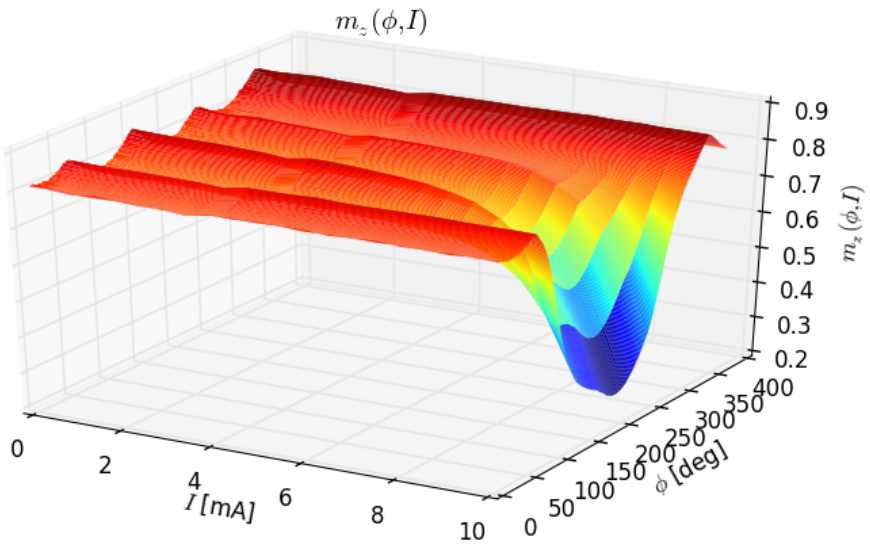


Figure 5.13: Magnetization along z as a function of current and $\phi$ for an intensity of the applied in plane field of 1.6T. With this value of the applied field there is not switching in the magnetization sign.

It is then subtracted from all the scans the $m_z$ resulting from a low current scan so that it is removed the contribution of the ordinary equilibrium position and is kept just the $\Delta m_z$ induced by SOT.

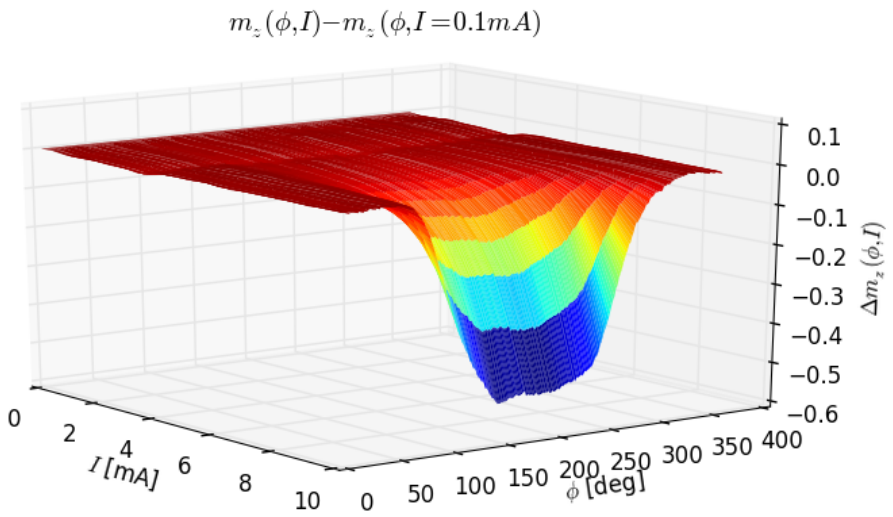


Figure 5.14: The figure shows $m_z(\phi, I) - m_z(\phi, I = 0.1mA)$. The maximum difference is achieved for an angle about $180^o$, considering that the current direction is placed at $90^o$, it is perpendicular to it.

The effective in plane field is estimated exactly as before and the results is shown in figure 5.15.
Strong non linear effect starts around 5 mA where the magnetization is perpendicular to the current. The effect is way higher than in the previous device and this could be due to the different expression that the effective field assume when the current direction changes.
Unfortunately it is difficult to quantitative compare the two different expression of the effective field obtained for the two different pattern (see equation 5.2.2.1 and 5.2.1.2) because of the lack of a precise definition of $m_x$ and $m_y$ already discussed. In order to distinguish between those quantities a suitable way would be to anneal the sample after the fabrication in a magnetic field so that the crystal would loose its four-fold symmetry and thus it will be possible to properly define $m_x$ and $m_y$.

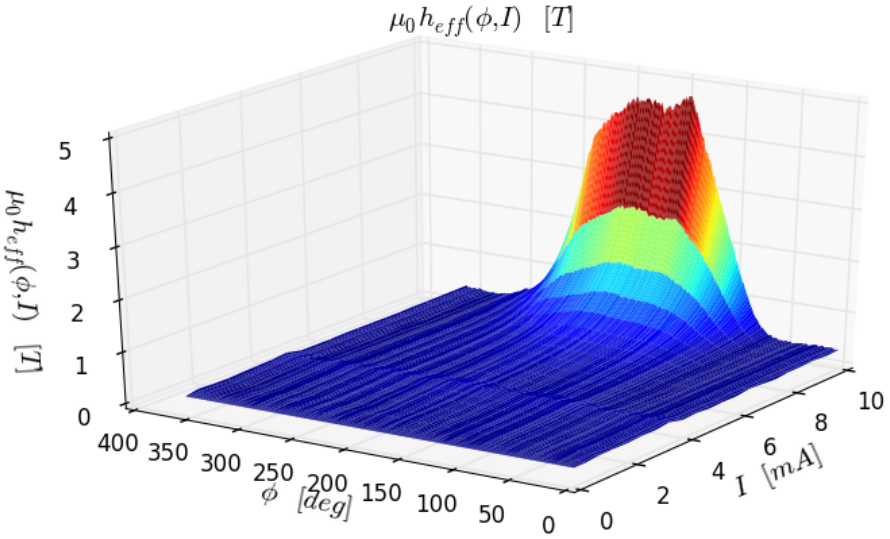


Figure 5.15: Effective in plane field.

At this point some comment on the symmetry of the non linear effective field is necessary. Observing both figure 5.15 and 5.10 it can be noticed that this effective field lacks of a particular symmetry, i.e. is neither even and neither odd in the magnetization direction.
Rewriting here, for simplicity, the two expressions of the effective field for the two different current directions a qualitative explanation can be obtained.

$$\mathbf{h}_{eff}^{[100]} = J_0 \begin{pmatrix} x_{FL} \\ x_{DL} m_z(\mathbf{J}) \\ x_{DL} m_y(\mathbf{J}) \end{pmatrix} \tag{5.2.2.2}$$

$$\mathbf{h}_{eff}^{[110]} = \frac{x_{FL} J_0}{\sqrt{2}} \begin{pmatrix} 1 \\ 1 \\ 0 \end{pmatrix} + \frac{x_{DL} J_0}{\sqrt{2}} \begin{pmatrix} m_z(\mathbf{J}) \\ m_z(\mathbf{J}) \\ m_x(\mathbf{J}) + m_y(\mathbf{J}) \end{pmatrix} \tag{5.2.2.3}$$

Observing equation 5.2.2.2 and 5.2.2.3 it can be noticed that the effect of the out of plane effective field should be antisymmetric as a function of the in plane magnetization direction. It is expected that the effective field changes sign but not intensity if $\phi \to \phi + \pi$. However considering that the in-plane magnetization depends on the current the effective field is not linear and in figure 5.16 it can be understood that depending on the magnetization

direction this dependence of the damping-like tensor from the current can enhance or damp the effective field.

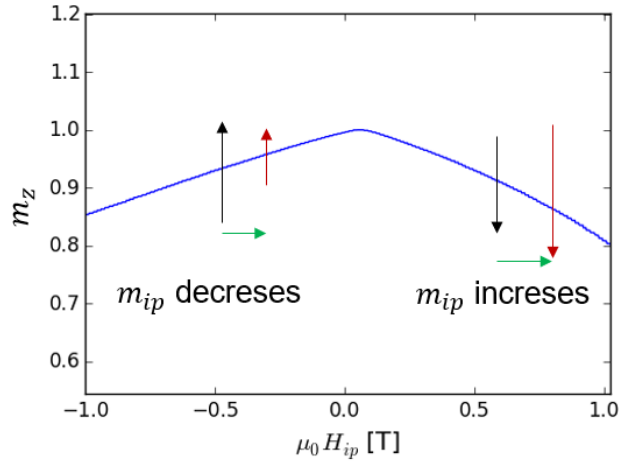


Figure 5.16: Qualitative explanation of the non-symmetric behavior of the non linear effective field. The black arrows represent the linear part of the out of plane effective field, the green arrows represent the change in the in plane magnetization and the red arrows represent thee non linear part of the effective field which is enhanced or damped by the change of the in pane magnetization due to the linear effective field.

In figure 5.16 it can be seen that on the left the effective field is positive so it, globally, decreases the in-plane magnetization and thus it decreases also the amplitude of the out of plane effective field itself. On the right, instead, the effective field is negative so it globally increases the in plane magnetization which give rise to an effective field which is enhanced.
This is just a qualitative model but it is able to explain such an absence of symmetry. This explanation could also provides a reason for the fact that the direction in which $\Delta\theta$ is maximum is perpendicular to the current direction. The linear SOT, as could be seen in figure 5.2, has a maximum $\Delta\theta$ which is not really perpendicular to the current direction, as it would be if the torque was just arising from the damping-like part of the tensor (see figure 4.1. This means that the ratio between filed-like and damping-like parameter has changed and, in non linear SOT, the damping-like part of the torque prevails on the field-like part. This is a further confirmation that the non linearity of SOT effect mainly arises from the fact that the magnetization could not be considered constant in the expression of the damping-like tensor, which is the unique one that depends on the magnetization.

# Chapter 6

# Conclusions and perspectives

During this thesis, Spin-orbit Torques effects in single layer were investigated and further understood. The effect was initially characterized at relatively low current density ($J_{max} \sim 2.5 \cdot 10^{10}\ A/m^2$) exploiting the Anomalous Hall signal recorded on the third harmonic.
By comparing accurate simulations performed in Python [36] with experimental results the two fundamental parameters that relate the current density to the effective field were estimated. In order to perform such comparison, it was necessary to carefully take into account all the effect that are superimposed to SOT on the third harmonic of the signal obtained, namely the current induced variation of $\sigma_{xx}$ and $\sigma_{xy}$.

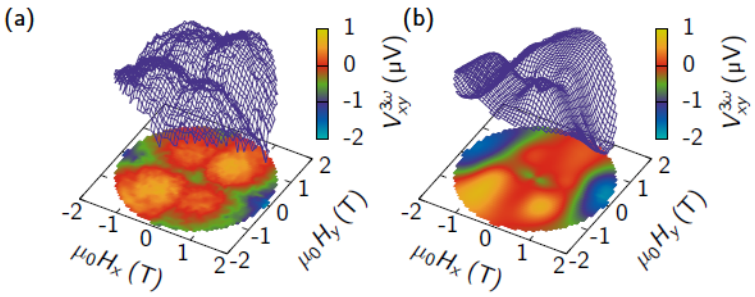


Figure 6.1: Comparison between the experimental signal recorded on the third harmonic (a) and the expected signal calculated using equation 5.1.1.1 with $x_{FL} = -15 \cdot 10^{-13} Tm^2A^{-1}$ and $x_{DL} = 50 \cdot 10^{-13} Tm^2A^{-1}$ (b).

The best agreement between experimental and expected signal is obtained for the following parameters:

$$x_{FL} = -15 \cdot 10^{-13}\ TA^{-1}m^2 \qquad x_{DL} = 50 \cdot 10^{-13}\ TA^{-1}m^2 \qquad (6.0.0.1)$$

It is interesting to observe this result in the light of a recent theoretical work published by R. Troncoso [19]. It was predicted that the symmetry of MRG if properly engineered to show an in-plane easy axis, could sustain SOT driven self-oscillations.
This means that the current flowing into the material due to SOT effect gains a polarization non-collinear with the magnetization. The magnetization itself starts to precede around the polarization's direction of the current. The interesting aspect of such a possibility is that being MRG a ferrimagnet, it would have a resonance frequency much greater than the resonance frequency obtained with ordinary ferromagnets.
These predicted oscillations are governed by the Landau-Lifshitz-Gilbert equation (2.1.6.1). The peculiarity is that the spin current is not generated externally and then injected into the material but is continuously polarized because of the symmetry of the lattice itself.
In particular, to guarantee the existence of self-oscillations, two conditions have to be respected. The first is that the effective field arising from the field-like part of SOT has to be stronger than the four-fold anysotropy, which results in $J_0 x_{FL} > \frac{2k_1^{'}}{\mu_0 M_{sat}}$ where $k_1^{'}$ is defined as in equation 3.2.4.2 and in our case is $\sim 0.1T$. This requires a current density $J > 7 \cdot 10^{10} A/m^2$. The second condition requires that the damping effect which tends to align the magnetization with the field is someway nullified by the damping-like torque. Considering a reasonable value for the Gilbert damping parameter $\alpha \simeq 0.01$ it turns out that the current density has to be $J > 10 \cdot 10^{10} A/m^2$.
The second significant result was related to the investigation of non-linear effects arising when the current density exceeds the value of $5 \cdot 10^10 A/m^2$.
In this regime a strongly non-linear SOT was observed, in both the current direction, parallel to [100] and to [110], the magnetization along the z-axis obtained at high current density was very different with respect to the magnetization obtained for low current.
This can be addressed just to the existence of a strongly non-linear Spin-Orbit torque effect.
In order to quantify the effective field the exploited model finally turned out to be incomplete. The effective field was estimated as an in-plane field, but the last measurements performed shows that it is most likely directed along the z-direction. This can be understood by observing figure 6.2.

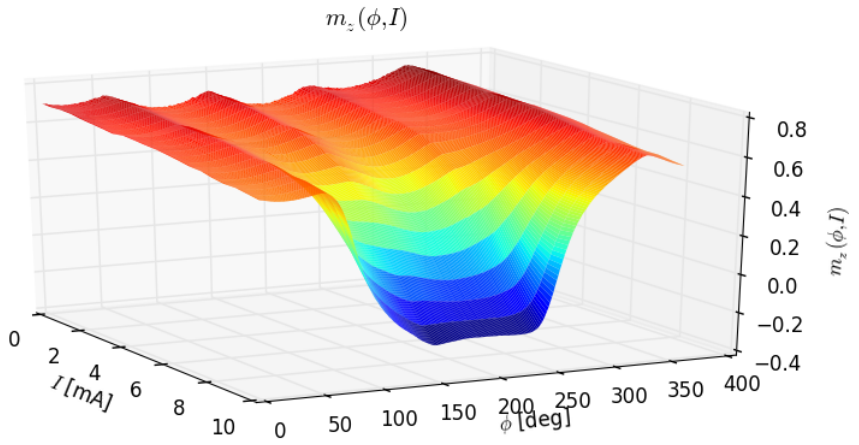


Figure 6.2: Normalized magnetization along the z-axis. For high values of the current, the magnetization is partially switched.

An important observation regarding the evolution of $m_z$ as a function of J and $\mathbf{M}/M_{sat}$ is that, after the magnetization crosses the plane of the sample and partially switches it, it is driven back to its initial value when the magnetization rotates of $180^o$. This is also confirmed by the fact that after the highest current density was injected a complete $\phi$ scan at low current was repeated. Observing a perfect match between the first and the last measurement, performed at the same current, it is confirmed that the magnetic state was not degraded during the experiment.
This suggests that with a DC current, it would be impossible to completely switch the magnetization of a sample because the effective field points upward or downward depending on the orientation of the magnetization. Thus, whenever the effective field is directed toward $(-z)$ the magnetization, while switching, it starts simultaneously to precede around the effective field and, as soon as it rotates of $180^o$ the direction of the effective field changes pointing toward $(+z)$.
Another important observation is that the orientation of the field depends both on the magnetization direction and on the sign of current. If the current is chosen to be a pulse, changing its direction exactly after the magnetization has completed a rotation of $180^o$, it would provide an effective field pointing toward the same direction during all the switching process.
Among the most urgent further plans there is the engineering of duration

and intensity of the pulse necessary to provide switching of a single layer of MRG. From a technological point of view, it would be a breakthrough to obtain an entirely electrically driven magnetic switching in a single layer without any interface effect.
Another interesting topic that has to be investigated as one of the next projects is the possibility of experimentally verify the existence of those SOT sustained self-oscillations. It is clearly difficult from a technological point of view to detect those oscillations because of their frequency which is in the terahertz gap. Namely, a gap of frequency between the maximum frequency achieved with classical electronics and the minimum operating frequency of photonics devices.
Already during some DC measurements, it was registered a sudden increase in the longitudinal resistance as a function of the DC current injected into MRG. This, suggests that beyond a certain threshold SOT driven self-oscillation are excited; thus, the sample is heated and the longitudinal resistance of the devise increases.
This is not a sufficient proof but, it makes such research topic quite interesting to be investigated.
Another essential topic to further investigate is related to the understanding of why a current injected parallel to the [110] crystallographic axis of MRG leads to a SOT much greater than along the [100] axis. In order to clarify this aspect, the capability to properly define $m_x$ and $m_y$ instead of classifying those as generic in-plane magnetization ($m_{ip}$) is needed.
This could be appropriately done breaking the four-fold symmetry annealing it into a magnetic field directed along x or y.
In conclusion, this work shows a fraction of the enormous potential that such a material possesses. It can combine a huge spin polarization with all the interesting properties of antiferromagnets and upon this, showing a symmetry which allows the existence of a strong SOT effect without the need of an extra layer to polarize the current or to break the symmetry.
Its potential suggests that there is still much work to be done in order to maximize the possibility related to such material.
This work has not the pretension of being considered fundamental from an academic or technology point of view but I hope that it could be of inspiration for someone who in future would like to further investigate some of the promising and very interesting phenomena that here are mentioned. I am very grateful to all the group of Magnetism and Spin Electronics of Trinity College Dublin. Here I found colleagues who were very helpful the whole time, always having the willingness of sharing as much as they could their experience and knowledge.

# List of Figures

# Bibliography


[1] M. N. Baibich, J. M. Broto, A. Fert, F. N. Van Dau, F. Petroff, P. Etienne, G. Creuzet, A. Friederich, and J. Chazelas, "Giant magnetoresistance of (001) fe/(001) cr magnetic superlattices," *Physical review letters*, vol. 61, no. 21, p. 2472, 1988.

[2] M. Julliere, "Tunneling between ferromagnetic films," *Physics letters A*, vol. 54, no. 3, pp. 225–226, 1975.

[3] J. Slonczewski, "Excitation of spin waves by an electric current," *Journal of Magnetism and Magnetic Materials*, vol. 195, no. 2, pp. L261–L268, 1999.

[4] L. Berger, "Emission of spin waves by a magnetic multilayer traversed by a current," *Physical Review B*, vol. 54, no. 13, p. 9353, 1996.

[5] J. Grollier, V. Cros, A. Hamzic, J.-M. George, H. Jaffrès, A. Fert, G. Faini, J. Ben Youssef, and H. Legall, "Spin-polarized current induced switching in co/cu/co pillars," *Applied Physics Letters*, vol. 78, no. 23, pp. 3663–3665, 2001.

[6] J.-E. Wegrowe, D. Kelly, T. Truong, P. Guittienne, and J.-P. Ansermet, "Magnetization reversal triggered by spin-polarized current in magnetic nanowires," *EPL (Europhysics Letters)*, vol. 56, no. 5, p. 748, 2001.

[7] M. D'yakonov and V. Perel, "Possibility of orienting electron spins with current," *Soviet Journal of Experimental and Theoretical Physics Letters*, vol. 13, p. 467, 1971.

[8] Y.-C. Lau, D. Betto, K. Rode, J. Coey, and P. Stamenov, "Spin–orbit torque switching without an external field using interlayer exchange coupling," *Nature nanotechnology*, vol. 11, no. 9, p. 758, 2016.

[9] L. Liu, T. Moriyama, D. Ralph, and R. Buhrman, "Spin-torque ferromagnetic resonance induced by the spin hall effect," *Physical review letters*, vol. 106, no. 3, p. 036601, 2011.

[10] H. Kurt, K. Rode, P. Stamenov, M. Venkatesan, Y.-C. Lau, E. Fonda, and J. Coey, "Cubic mn 2 ga thin films: Crossing the spin gap with ruthenium," *Physical review letters*, vol. 112, no. 2, p. 027201, 2014.

[11] J. Železnỳ, H. Gao, A. Manchon, F. Freimuth, Y. Mokrousov, J. Zemen, J. Mašek, J. Sinova, and T. Jungwirth, "Spin-orbit torques in locally and globally noncentrosymmetric crystals: Antiferromagnets and ferromagnets," *Physical Review B*, vol. 95, no. 1, p. 014403, 2017.

[12] J. C. Maxwell, *The Scientific Papers of James Clerk Maxwell...*, vol. 2. University Press, 1890.

[13] N. Mazzoldi Paolo, "Elementi di fisica 2-elettromagnetismo e onde," 2008.

[14] J. M. Coey, *Magnetism and magnetic materials*. Cambridge university press, 2010.

[15] F. Ciccacci, *Fondamenti di fisica atomica e quantistica*. EdiSES, 2012.

[16] S. Blundell, "Magnetism in condensed matter," 2003.

[17] A. Aharoni *et al.*, *Introduction to the Theory of Ferromagnetism*, vol. 109. Clarendon Press, 2000.

[18] S. Zhang and S. S.-L. Zhang, "Generalization of the landau-lifshitz-gilbert equation for conducting ferromagnets," *Physical review letters*, vol. 102, no. 8, p. 086601, 2009.

[19] R. E. Troncoso, K. Rode, P. Stamenov, J. M. D. Coey, and A. Brataas, "Antiferromagnetic single-layer spin-orbit torque oscillators," *Physical Review B*, vol. 99, no. 5, p. 054433, 2019.

[20] E. Hall, "On a new action of the magnet on electric currents," *American Journal of Science*, no. 111, pp. 200–205, 1880.

[21] J. Smit, "Magnetoresistance of ferromagnetic metals and alloys at low temperatures," *Physica*, vol. 17, no. 6, pp. 612–627, 1951.

[22] N. Nagaosa, J. Sinova, S. Onoda, A. H. MacDonald, and N. P. Ong, "Anomalous hall effect," *Reviews of modern physics*, vol. 82, no. 2, p. 1539, 2010.

[23] J. Smit, "The spontaneous hall effect in ferromagnetics i," *Physica*, vol. 21, no. 6-10, pp. 877–887, 1955.

[24] J. Smit, "The spontaneous hall effect in ferromagnetics ii," *Physica*, vol. 24, no. 1-5, pp. 39–51, 1958.

[25] R. Karplus and J. Luttinger, "Hall effect in ferromagnetics," *Physical Review*, vol. 95, no. 5, p. 1154, 1954.

[26] K. Garello, F. Yasin, H. Hody, S. Couet, L. Souriau, S. Sharifi, J. Swerts, R. Carpenter, S. Rao, W. Kim, *et al.*, "Manufacturable 300mm platform solution for field-free switching sot-mram," in *2019 Symposium on VLSI Circuits*, pp. T194–T195, IEEE, 2019.

[27] P. Gambardella and I. M. Miron, "Current-induced spin–orbit torques," *Philosophical Transactions of the Royal Society A: Mathematical, Physical and Engineering Sciences*, vol. 369, no. 1948, pp. 3175–3197, 2011.

[28] E. Rashba, "Symmetry of energy bands in crystals of wurtzite type. 1. symmetry of bands disregarding spin-orbit interaction," *Soviet Physics-Solid State*, vol. 1, no. 3, pp. 368–380, 1959.

[29] G. Dresselhaus, "Spin-orbit coupling effects in zinc blende structures," *Physical Review*, vol. 100, no. 2, p. 580, 1955.

[30] M. Kepenekian and J. Even, "Rashba and dresselhaus couplings in halide perovskites: Accomplishments and opportunities for spintronics and spin–orbitronics," *The journal of physical chemistry letters*, vol. 8, no. 14, pp. 3362–3370, 2017.

[31] M. Studer, M. Walser, S. Baer, H. Rusterholz, S. Schön, D. Schuh, W. Wegscheider, K. Ensslin, and G. Salis, "Role of linear and cubic terms for drift-induced dresselhaus spin-orbit splitting in a two-dimensional electron gas," *Physical Review B*, vol. 82, no. 23, p. 235320, 2010.

[32] R. R. Birss *et al.*, *Symmetry and magnetism*, vol. 863. North-Holland Amsterdam, 1964.

[33] H. Van Leuken and R. De Groot, "Half-metallic antiferromagnets," *Physical review letters*, vol. 74, no. 7, p. 1171, 1995.

[34] D. Betto, K. Rode, N. Thiyagarajah, Y.-C. Lau, K. Borisov, G. Atcheson, M. Žic, T. Archer, P. Stamenov, and J. Coey, "The zero-moment half metal: How could it change spin electronics?," *AIP Advances*, vol. 6, no. 5, p. 055601, 2016.

[35] K. Borisov, D. Betto, Y.-C. Lau, C. Fowley, A. Titova, N. Thiyagarajah, G. Atcheson, J. Lindner, A. Deac, J. Coey, *et al.*, "Tunnelling magnetoresistance of the half-metallic compensated ferrimagnet mn2ru x ga," *Applied Physics Letters*, vol. 108, no. 19, p. 192407, 2016.

[36] S. Lenne, Y.-C. Lau, A. Jha, G. P. Atcheson, R. E. Troncoso, A. Brataas, M. Hayashi, J. Coey, P. Stamenov, and K. Rode, "Giant spin-orbit torque in a single ferrimagnetic metal layer," *arXiv preprint arXiv:1903.04432*, 2019.

# Acknowledgments

During the months spent in the physical laboratories of Trinity College Dublin I had the opportunity to actively participate in a cutting edge research project.
Such experience was for me the first of its kind, it allows me to discover the difficult but very fascinating world of scientific research.
Many people deserve my thanks and gratitude to have encouraged me during this period, starting from prof. Riccardo Bertacco who suggested me to contact the group of Magnetism and Spin Electronics at Trinity College Dublin.
I thank prof. Michael Coey to have accepted me into his group and for being from the first moment extremely willing to discuss with me about the possible thesis project that could have been performed in the group.
The person who mostly inspired and taught me during the past nine months is Dr. Karsten Rode. He was always available to share his knowledge but also to listen to other opinions, ideas and discuss about it. I really appreciated the fact that he always allowed me to follow my ideas and to eventually realize if they were true or wrong. This was the best way to make me understand what it really means to perform scientific research.
I am very grateful also to prof. Plamen Stamenov who was very patient during all our discussion about the experimental results and extremely human talking with me about my future plans.
I think that the responsibility of having created such a positive work environment belongs to the whole group, to the willingness of every member of sharing his knowledge and his experience.
I thank Gwenael and Tzolt for the help with all the machines, Jean for the discussions about physics, Niclas for having showed me how to deal with MOKE microscopy, Kat for the frequent suggestion and chat, Stephen for being very patient while showing me how to deal with UV-lithography, Ross, Tim, Brian, Jack, Shruty, Zexiang and Ajay for the time spent together in the lab and outside. In the end I thank Simon for the help about the management of the software and for the continuous sharing of opinions about physics or everything else.

Foto di gruppo 2018.
Back (from left): Plamen, Nigel, Niclas, Stephen, Venkie, Karsten, Jean, Simon, Gwenael, Lorenzo, Eleanor and Mike.
Front (from left): Akshara, Fenjuan, Rui, Ajay, Jane, Alexandra, Kat.

But my life is much more than my experience in TCD, I would like to thank all the people that have contributed to make me the person that I am today. My parents who always supported me, my grandparents who gave me all their love and wisdom and all the rest of my family.
I thank my friend to have grown with me and to having kept our friendship continuously growing since we were fourteen.
Finally, a special thank to who since five years share every day of her life with me.

*Lorenzo Locatelli*